International Journal of
Molecular Sciences

MDPI

Review

Nanosecond Pulsed Electric Field (nsPEF): Opening the Biotechnological Pandora's Box

Alvaro R. Ruiz-Fernández [1,2,*], Leonardo Campos [1,2], Sebastian E. Gutierrez-Maldonado [1,2], Gonzalo Núñez [1], Felipe Villanelo [1,2] and Tomas Perez-Acle [1,2,*]

[1] Computational Biology Lab, Centro Científico y Tecnológico de Excelencia Ciencia & Vida, Fundación Ciencia & Vida, Santiago 7780272, Chile; leocampos@dlab.cl (L.C.); sebastian@dlab.cl (S.E.G.-M.); gonzalo.nunez@dlab.cl (G.N.); felipe@dlab.cl (F.V.)
[2] Facultad de Ingeniería y Tecnología, Universidad San Sebastian, Bellavista 7, Santiago 8420524, Chile
* Correspondence: aruiz@dlab.cl (A.R.R.-F.); tomas@dlab.cl (T.P.-A.)

Abstract: Nanosecond Pulsed Electric Field (nsPEF) is an electrostimulation technique first developed in 1995; nsPEF requires the delivery of a series of pulses of high electric fields in the order of nanoseconds into biological tissues or cells. They primary effects in cells is the formation of membrane nanopores and the activation of ionic channels, leading to an incremental increase in cytoplasmic Ca^{2+} concentration, which triggers a signaling cascade producing a variety of effects: from apoptosis up to cell differentiation and proliferation. Further, nsPEF may affect organelles, making nsPEF a unique tool to manipulate and study cells. This technique is exploited in a broad spectrum of applications, such as: sterilization in the food industry, seed germination, anti-parasitic effects, wound healing, increased immune response, activation of neurons and myocites, cell proliferation, cellular phenotype manipulation, modulation of gene expression, and as a novel cancer treatment. This review thoroughly explores both nsPEF's history and applications, with emphasis on the cellular effects from a biophysics perspective, highlighting the role of ionic channels as a mechanistic driver of the increase in cytoplasmic Ca^{2+} concentration.

Keywords: nsPEF; NPS; nanopores; ionic channels; medical devices; cancer

Citation: Ruiz-Fernández, A.R.; Campos, L.; Gutierrez-Maldonado, S.E.; Núñez, G.; Villanelo, F.; Perez-Acle, T. Nanosecond Pulsed Electric Field (nsPEF): Opening the Biotechnological Pandora's Box. *Int. J. Mol. Sci.* **2022**, *23*, 6158. https://doi.org/10.3390/ijms23116158

Academic Editor: Dongho Kim

Received: 28 April 2022
Accepted: 23 May 2022
Published: 31 May 2022

1. A Brief History on the Development of Electric Pulses Technology

The use of electricity in humans can be traced back to the 18th century, when tissue damage was observed after the application of electric fields [1]. Despite the occurrence of lesions on the skin of humans and animals after exposure to electric sparks, the mechanism of action was far from being understood. Much latter, circa 1982, Neumann et al. achieved the first DNA transfection into cells [2] by applying a protocol including an electric field of 8 kV/cm for 5 µs, inducing a phenomenon in the cell membrane they termed *electroporation*. Almost a decade later, Pakhomov et al. demonstrated that the application of electric fields on cells creates water-filled lipid nanopores forming a stable, ion channel-like conduction pathway in the cell membrane [3]. Denoting its appropriateness, the definition of electroporation has remained intact for over 30 years: "electroporation is the transient loss of semi-permeability of cell membranes under the application of electric pulses, leading to ion leakage, the escape of metabolites, and increased cell-uptake of drugs, molecular probes, and DNA" [4]. Since its remote origins, this technology is nowadays widely used for several applications other than DNA transfection, such as electrochemotherapy [5,6], tissue ablation [7,8], extraction of chemical compounds [9,10], and microbial inactivation for food preservation [11], among others. The next significant step along the historical evolution of the application of electric pulses to biological systems occurred in 1995, when Schoenbach et al. developed a technique to generate high intensity nano-pulsed electric fields, on the order of 6.45 kV/cm with a duration ~700 ns, to treat natural water used in industrial cooling systems [12]. This technique is nowadays known by the academic

community either as nanosecond Pulsed Electric Field (nsPEF) or Nano Pulse Stimulation (NPS). Later on, Schoenbach started a longstanding collaboration with Stephen J. Beebe; together they pioneered the nsPEF field, studying systematically its effects in cells through both theoretical and experimental approaches, giving this technique a new spectrum of applicability (see Section 7). By stepping into the sub-nanosecond realm, inspired by a note from Carl E. Baum in 2005 and later published in 2007 [13], Heeren et al. used an impulse radiating antenna (IRA) instead of electrodes to deliver an electric pulse with a peak amplitude of about 250 kV and with a pulse-width of ~600 ps [14]. This development added two main advantages to the field: the capability of delivering an electric pulse in the order of picoseconds, and the ability to target deeper body tissues, allowing the application of nsPEF in vivo. Figure 1 summarizes the main events through time in the development of nsPEF technology.

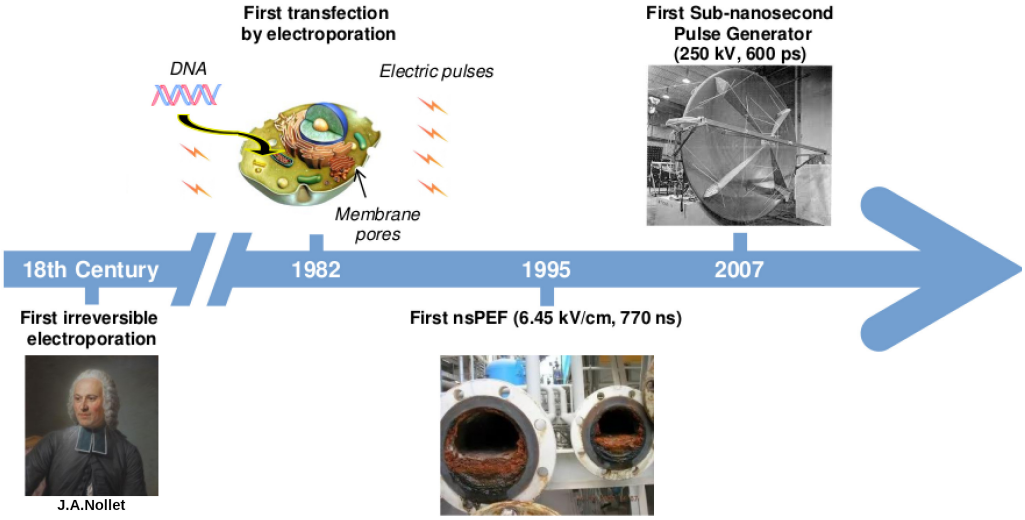

Figure 1. Timeline of main events in the development of electric pulse technology. The first application of electric pulses was recorded in 1754 with the experiments performed by J. A. Nollet. Two centuries later, in 1982, E. Neumann et al. [2] coined the term electroporation to describe the use of electric pulses to create membrane pores allowing the insertion of genetic material into cells. Afterwards, in 1995, Schoenbach et al. [12] developed the first nsPEF technology to prevent biofouling of cooling systems. Lately, the construction of an IRA in 2007 by Heeren et al. [13], allowed the application of sub-nanosecond pulses.

2. nsPEF and Ca^{2+}-Mediated Apoptosis: An Evolutionary Prespective

Despite a long-dated and active debate, abundant literature suggests that one of the main cellular consequence due to the application of nsPEF in cells is the increase in the cytoplasmic concentration of Ca^{2+}, impacting multiple cellular pathways (see Section 3).

Accumulated knowledge from molecular biology allows us to better understand the relationship between inner cell Ca^{2+} homeostasis and its role in the evolution of the eukaryotic cells [15]. A paleobiological hypothesis postulates that the prehistoric alkaline ocean contained extremely low Ca^{2+} concentration [16]: i.e., life emerged from a calcium-free medium (Figure 2). This hypothesis agrees with the fact that all life forms on Earth are supported by cells containing low cytoplasmic Ca^{2+} concentrations, a necessary condition to not perturb ATP metabolism since phosphate precipitates in the presence of Ca^{2+} [17]. Eukaryotic cells can achieve cytoplasmic nanomolar concentrations of Ca^{2+} by distributing it in organelles. These internal reservoirs allows a fast and focal release of Ca^{2+} at specific cell sites, generating a variety of cellular signals as a consequence of its reversible binding to calcium-binding proteins (CaBP) [18,19]. Thus, evolution took advantage of the increase of calcium in the internal media by turning calcium into a pleiotropic second messenger [20]. Calcium's evolutionary protagonism is highlighted by an increase in the number of CaBP along evolution, which rises from nearly 70 in bacteria to more than 3600

in mammals [21,22], therefore improving the ability of eukaryotic cells to fine tune Ca^{2+} signals [23]. In this regard, nsPEF may represent a technological key suitable to open the Ca^{2+} Pandora's box in cells, turning over the recalcitrant evolutionary path of life tending to exquisitely regulate the internal Ca^{2+} concentration and providing us with a unique tool to manipulate cellular metabolism.

Controlling cell homeostasis due to the rise in internal cytoplasmic Ca^{2+} concentration produces massive consequences to cell fate: from either proliferation and differentiation to apoptosis. Cases of cell proliferation induced by the application of nsPEF are scarce, and the underlying mechanism is still a matter of discussion. Using microalgae, Buchmann et al. hypothesized through proteomic analysis that this proliferation may be the result of the activation of some stress response pathway [24]. They found that two proteins were overexpressed after the application of nsPEF, one of them being the Na^+/Ca^{2+} exchanger/integrin-β4. Integrins are related to growth stimulation as they signal guanine nucleotide-binding proteins [25]. The overexpression of these proteins agrees with the abiotic stress response in plants, which involves Ca^{2+} as an essential second messenger [26]. On the other hand, apoptosis is also triggered by nsPEF, a field with exponential growth given its application in cancer treatment [27]. Despite an abundance of experimental data, the exact underlying cellular mechanisms controlling this process are still a matter of debate. However, as mentioned before, available evidence shows that the primary effect of the application of nsPEF in cells is the sudden increase in cytoplasmic Ca^{2+} concentration [28,29].

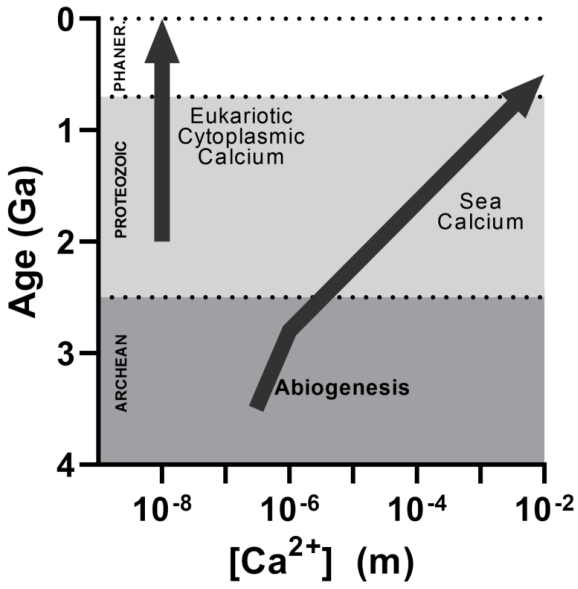

Figure 2. Calcium concentration as a function of time in the sea and in cytoplasmic eukaryotic cells.

3. nsPEF Action Mechanism: A Deep Controversy

Given the lack of an experimental setup able to follow cell changes on the nanosecond scale, and despite the substantial advances in the field during the past 15 years, the mechanism through which nsPEF increases cytosolic Ca^{2+} concentration is still a matter of discussion. Previous reports suggested that nsPEF produces similar effects in the cell membrane as those that occur with electroporation, albeit two main differences: the size of the pores induced in the membrane (termed nanopores) and their location [30–32]. Even though the induction of nanopores by nsPEF has not yet been experimentally confirmed, theoretical knowledge provides suitable foundations supporting this hypothesis. The application of an electric field with the necessary magnitude to reach voltage differences of one order of magnitude above the resting potential of the cytoplasmic membrane should be enough to transiently induce nanopores [33]. This is exactly the case in experimental

nsPEF setups [34]. From the biophysical point of view, the electric field ($\vec{E}$) resulting from a voltage difference (ΔV) ($\vec{E} = \Delta V/d$, where d is membrane thickness) across the cell membrane generates a force over charged atoms ($\vec{F} = q\vec{E}$, where q is the charge) that may perturb membrane integrity. In fact, Vernier et al. observed from Molecular Dynamics (MD) simulations that pore formation was due to electrophoretic migration of charged phospholipids initiated by the field-driven alignment of water dipoles at the membrane interface [33]. This finding was further supported by experimental evidence showing that negatively charged phosphatidylserine migration from the internal membrane leaflet to the external one occurred as a result of the application of a nanosecond pulse above two MV/m [35,36]. Thus, available evidence suggest that the increase in cytoplasmic Ca^{2+} concentration produced by the application of nsPEF could be due to the formation of membrane nanopores. However, an important question remained: are these nanopores located in the plasmatic and/or the internal membranes? The first studies focused on answering this question suggested that the application of nsPEF indeed affects the internal membranes. Therefore, the increase in cytoplasmic Ca^{2+} concentration could be the result of this ion being released from internal organelles such as the sarcoplasmic reticulum [32,37,38]. This evidence provided an inflection point in cell manipulation: nsPEF was cataloged as the first non-invasive, drug-free technique affecting organelles without altering the cytoplasmic membrane [39,40].

Albeit slowly, since 2005, new data have tipped the evidence scale towards the recognition that the application of nsPEF may produce larger effects on the cytoplasmic membrane than on internal ones. Nowadays, a large body of evidence supports the notion that the application of nsPEF produces effects mostly on the plasma membranes, but not necessarily through nanopore formation. Table 1 briefly summarizes some studies focused on localizing nsPEF-induced nanopores. For further references regarding the formation of nanopores on the internal membranes, please see [32,41–46].

Table 1. Examples of both theoretical and experimental studies exploring nanopore formation upon the application of nsPEF.

nsPEF (kV/cm)	Pulse Time (ns)	Cell Line Used	Observed Effect	Year and Citation
13.5	50	HL-60 leukemia cells	nsPEF affects the nucleus but not the plasma membrane	1997 [47]
60	60	Theoretical cell model including representations of several organelles	nsPEF goes through cell membrane, extensively penetrating organelles	2006 [48]
~150	10–100	Sp2, mouse murine myeloma cells	The cytoplasmic membrane is capable of withstanding nsPEF application, suggesting that permeabilization of organelles is the main effect	2001 [49]
53	60	Human neutrophil and eosinophil cells	nsPEF induces poration of eosinophils' intracellular granules. This occurs without permanent disruption of the cytoplasmic membrane. Of note, neutrophils show no changes	2001 [50]
4–15	60	HL-60 leukemia cells	nsPEF induces a rise in cytoplasmic Ca^{2+} concentration without incorporation of external propidium iodide and using a Ca^{2+}-free media, suggesting no cell membrane poration, but poration of internal membranes	2004 [51]
20–80	4	Chromaffin cells	nsPEF induces a rise in cytoplasmic Ca^{2+} concentration not affected by the depletion of intracellular calcium storage with either caffeine or thapsigargin, being completely prevented by the presence of EGTA (a Ca^{2+} chelator) in the extracellular medium	2008 [52]
22–24	60	GH3 murine pituitary, PC-12 murine adrenal, and Jurkat cells (immortalized human T-lymphocytes)	nsPEF induces a long-lasting effect (~100 s) on cytoplasmic membrane permeabilization that can be monitored by patch-clamp	2007 [53]
2.4–4.8	600	GH3 and CHO-K1 Chinese hamster ovary cells	nsPEF induces an incremental increase in cell conductance, attributed to the formation of ion-channel-like nanopores in the cytoplasmic membrane with a maximum width of 1 nm in both studied cell lines. The size was proposed because the membrane remained mostly impermeable to propidium iodine	2009 [3]

Despite its crucial role maintaining the integrity and fluidity of cellular membranes, and its being the most abundant molecule in biological membranes after phospholipids [54–79], the role of cholesterol during the formation of nanopores is poorly understood. Early experimental in vivo and in vitro studies, as well as theoretical approaches, were designed

to explore the effects of the cholesterol composition of cellular membranes during nsPEF-induced electroporation [80–84]. Conductance analyses of electroporated membranes indicate that formed pores may have diameters between 0.9 nm and 10.6 nm depending on the applied current and ionic strength of the media [85,86]. On the other hand, the small polar head and large hydrophobic core of cholesterol decreases the probability of pore formation by diminishing cellular membrane conductance [87,88]. Trying to get insight of the structure and dynamics of nanopore formation using molecular simulations, nsPEF application was simulated by a constant electric field on a membrane bilayer. Using pure 1-palmitoyl-2-oleoyl-sn-glycero-3-phosphocholine (POPC) membranes, $\vec{E}$ = 0.2 V/nm was needed to induce a nanopore after 13.6 ns of simulation. In contrast, a higher electric field of $\vec{E}$ = 0.35 V/nm and a larger simulation time (33.5 ns) was requited to induce a nanopore when the authors used a membrane with POPC-50%M/cholesterol–50%M [84]. These data suggest that the presence of cholesterol in the membrane provides higher stability during the application of nsPEF. Of note, CHO-K1 cells having a cholesterol-depleted membrane by using methyl-β–cyclodextrin (MβCD) were more sensitive to nanopore formation after the application of nsPEF pulses (10–150 kV/cm, 10–600 ns, up to 150 pulses) [89]. In [90], using the same nsPEF protocol and cell line as before, the authors used 3-(4,5-dimethylthiazol-2-yl)-2,5-diphenyl tetrazolium bromide (MTT) to evaluate toxicity. A linear relationship between the sensitivity to nsPEF to the amount of cholesterol removed with MβCD, and the incorporation of MTT was found [89,90], denoting the importance of cholesterol to maintain the structure and integrity of cell membranes under nsPEF application.

4. Dissecting the Biophysical Principles behind nsPEF's Effects

In general terms, nsPEF can be classified as non-invasive electrostimulation [39,40]. Its application does not involve the absorption of energy by molecules, except for kinetic energy, as is the case of standard ionizing radiation techniques such as X-rays, NMR, PET, and cancer radiotherapy. As mentioned before, the main effect of the application of nsPEF into cells is the movement of charged species under the influence of the force resulting from the potential difference across the cell membrane. Therefore, this phenomenon can be classified between electrostatic and electrodynamics, because the nanometric timescale of the applied pulse creates an electric field that is changing in time over the cell membrane. An excellent review by Schoenbach et al. dives deeper into these matters [91].

Despite the lack of an explanatory consensus regarding how nsPEF affects either the plasmatic and/or the internal membranes, a common knowledge base has accumulated indicating that the location of nsPEF's effects could be related to its intensity and time interval and the characteristic membrane charging time. It is important to address that the $\vec{E}$ delivered by an nsPEF protocol would not instantaneously increase the membrane $\vec{E}$. As in any RC circuit, a capacitor (i.e., the cytoplasmic membrane) does not fully charge until a certain time lapses, which is related to the RC time-constant ($\tau = RC$, where R is the resistance and C the capacitor's capacitance). In the comparative case of a cell, R represents the value given by the cell's surrounding medium. The equation describing the capacitor's voltage increment over time in an RC circuit is:

$$V(t) = V_0 e^{-t/\tau} \quad (1)$$

where $V(t)$ is the capacitor voltage at a certain time t, V_0 is the capacitor voltage at time $t = 0$, and $t = \tau$ is the time when the capacitor reaches around 63% of its charge capacity, almost reaching its maximum capacity around 4τ.

Theoretical approaches available in the literature have described the increase in membrane voltage as a function of time, and the dependency of the membrane time-constant (τ_m) with the surrounding media [92] as described by:

$$V_g(t) = 1.5 a E_0 cos\theta (1 - e^{-t/\tau_m}) \quad (2)$$

where $V_g(t)$ is the voltage difference across the cytoplasmic membrane of a spherical cell, a is the cell radius, θ is the polar angle measured with respect to the electric field $\vec{E}_0$, and τ_m is the relaxation time-constant [49] which is also known as membrane charge time, charging time-constant [35,47,50,93,94], or charging time [27,48,50]. It is well known that Equation (2) describes exponential growth for $V_g(t)$, with a limit of $1.5aE_0cos\theta$.

On the other hand, the constant τ_m can be defined by Equation (3) as follows:

$$\tau_m = aC_m(1/2\sigma_e + 1/\sigma_i) \quad (3)$$

where C_m is the membrane capacitance per unit of area, σ_e is the external conductivity, and σ_i is the internal conductivity. In mammalian cells, τ_m is characterized around ~100 ns [35,95]. Of note, τ_m does not represent the membrane charge time; it is the time when the membrane reaches 63% of its charge capacity, reaching 95% in 3τ [93]. As noted, a controversy arises when considering that the application of nsPEF protocols using time intervals far below the membrane τ_m are also capable of producing nanopores. Moreover, as seen in Table 1, no clear relationship between the intensity, duration, and the area of impact in the cell can be established.

A theoretical analysis could shed some lights on this controversy; either the application of nsPEF affects the plasmatic membrane, the inner organelle membranes, or both. If the cell is considered, for the sake of simplicity, as a solid metal and conducting sphere, the electrons contained in the sphere should migrate to the anode when an external electric field is applied. After a characteristic amount of time, this continuous migration of electrons should result in an asymmetric charge distribution, creating a self-induced electric field around the sphere (the reaction field) that could nullify the external electric field, resulting in a zero electric field inside the sphere. A similar phenomenon may occur in cells due to the application of nsPEF, but instead of electron movement, there are ions moving around creating equilibrium in the charge distribution to be reached in a much longer time (Figure 3). As the characteristic time to nullify the external electric field in cells is in the order of microseconds or even milliseconds [96] during standard electroporation, where pulses last longer, the reaction field in the cells should equilibrate, and charge relocation should cease. This is not the case when nsPEF is applied because the pulse duration is in the nanosecond scale, and therefore the movement of charges is not able to reach the necessary equilibrium so as to nullify the applied external electric field. Hence, internal charges will continue to move by the influence of the external electric field induced by the application of the nsPEF, continuously perturbing the structure and dynamics of internal structures in the cell. Consequently, with this analysis, long-lasting nsPEF protocols will eventually perturb not only the internal structures of the cell but also the plasma membrane, as can be seen in Table 1.

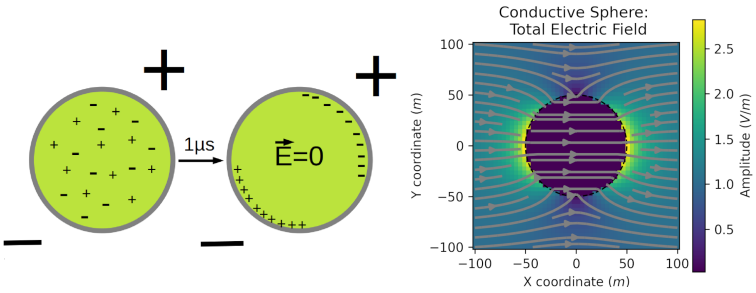

Figure 3. Schematic representation of the movement of charges inside a simplified model of a cell containing positive and negative charges under the application of an external electric field. After a suitable elapsed time, for instance 1 μs, the movement of charges reaches an equilibrium, resulting in the electric field inside the cell being nullified. Right panel showing the total electric field extracted from https://em.geosci.xyz (accessed on 27 April 2022).

5. It's All about Pores? In the Shade of Voltage-Gated Ion Channels

5.1. Voltage-Gated Channel (VGC) Activation Mechanism

Despite the abundant literature suggesting that the primary effect of the application of nsPEF protocols in cells should be the formation of nanopores, available evidence indicates that the activation of voltage-gated ion channels is also a relevant effect (see Section 5). However, it is also important to recognize the controversy arising from the significant differences between the time scales of the application of nsPEF protocols, in the order of nanoseconds, and the characteristic activation time of ion channels, in the order of ms [97,98]. To further understand the implications behind this time scale controversy, it is first necessary to explore with greater details the activation mechanisms of VGCs. During VGC activation, displacement of the charges tethered to the Voltage Sensing Domain (VSD) gives rise to transient gating currents. Kinetics indicate that during VGC activation, the VSD undergoes a complex conformational change that encompasses many transitions [99–101]. Four main models have been proposed to rationalize the transfer of charge during VGC activation, all of them associated with the motion of the S4 helix [102,103]. These four models are called the *helical screw-sliding* model [104,105], *kinetic* model [106], *paddle* model [107] introduced following the publication of the K^+ channel (KvAP) structure [108], and *transport* model [109].

- ***Helical screw-sliding model***: This simple model proposes that the S4 helix is responsible for maintaining the pore in a closed state during the resting potential. This is achieved by displacement of the positively charged S4 helix attracted by negative charges close to the cytoplasm. During depolarization, this attraction would vanish, and the system would return to a 60° rotation of S4 around its geometric axis. This rotation is accompanied by a vertical displacement of 5 Å to the extracellular side. According to this model, the positive residues of the S4 helix form salt bridges with acidic residues on opposite transmembrane segments. This model was based on the sodium channel transmembrane structure determined for an *Electrophorus electricus* channel [110,111]. Charge reversal mutagenesis [112] and disulfide linking [113] were used to probe charge interactions within the VSD of different VGCs. These works demonstrated the existence of a sequential ion pair formation involving S4 basic residues, typical on this type of channels. These interactions were key to conformational changes of the VSD upon VGC voltage activation. Subsequent works demonstrated similar key interactions required to characterize VGC activation in a more detailed fashion. Using site mutagenesis, two negatively-charged residues and a highly conserved one were identified as "catalyzers" of the transfer of each of the VSD basic residues across the membrane electric field [114]. This cluster of residues is known as the *Charge Transfer Center*.
- ***Kinetic model***: In this model, at hyperpolarizing potentials, the basic amino acid residues of S4 are connected with an intracellular water crevice, maintaining the channel in a closed state. Upon depolarization, the S4 helix tilts and rotates 180° around its geometric axis, allowing it to be connected to an extracellular water crevice. This conformational change of the S4 helix pulls the intracellular side of the S5 transmembrane helix, leading to a rotation and pulling of the intracellular section of the S6 helix, which forms the pore, opening the channel. This model was proposed for mammalian ion channels based on the gating mechanism of the prokaryotic KcSa potassium channel [106,115,116].
- ***Paddle model***: The paddle in this model circumscribes to the helix-turn-helix motif between the S3 and S4 helices. The paddle moves its center of mass nearly 20 Å and tilts towards a more vertical orientation. Since each paddle in the four VSDs of the VGC contains four arginine residues, with one electron charge unit per arginine [117,118], their displacement would account for the total gating charge in the Shaker K^+ channel of 12–14 electrons (3.0–3.5 electrons per subunit) [117–119]. Ionic interaction with S2 and S3 helices would stabilize the movement of paddle charges. The S4–S5 linker is pulled to open the VGC pore as a result of the paddle movement.

- ***Transport model***: Experimental observations on the Shaker K^+ channel with fluorescent resonance energy transfer (FRET) concluded that the S4 helix does not move during channel activation. To explain this observation, the same author of the kinetic model proposed that the voltage gating is due to a transmembrane field rearrangement. In this rearrangement, VSD's water crevice plays a key role. In this model, the S4 helix gyrates 45° around its geometric axis and has a vertical shift of less than 2 Å. The S4 turn relocates the S4 charges, reverberating from a deep, internally facing aqueous crevice in the closed state to an external water crevice when it opens. This model is supported by experimental evidence of a proton-conducting pore in a mutant Shaker channel in the closed state [120], the strong dependence of gating charge quantity on intracellular ionic strength, and the measurement of an amplified membrane electric field near the second gating-charge amino acid residue [121].

5.2. The Time-Scale Controversy behind Ion Channel Activation by nsPEF Protocols: The Role of MD Simulations

As noted in the previous section, regardless of the actual mechanism for the activation of VGCs, the extensive conformational changes occurring during the activation of VGCs require elapsed times in the order of ms [97,98]. Therefore, new data are needed to provide a biophysically sound explanation for the activation of ion channels in the nanosecond time scale, as occurs with nsPEF. For this task, molecular modeling and MD emerge as suitable tools to provide an atom-based description of the structural and dynamical changes occurring in ion channels under the application of nsPEF protocols.

MD results strongly suggest that the conformational changes at the VSD proceed after the ion channel closes, providing new evidence to support the *kinetic model* [122]. Recently released X-ray structures of ion channels also support the *kinetic model* through the observation that their VSD structures in the active state of the channels are linked to a closed pore domain [123,124]. Moreover, MD results able to reach a resting state of the channels exhibit a VSD conformation that is in agreement with the *kinetic model* [125–130]. Despite the agreement between these results, the large negative voltages used during the MD protocols must be taken with caution because there are neither in vivo nor in vitro experiments performed under the same conditions.

Another observation from long MD simulations is that the pore domain has to undergo a de-wetting process of its intracellular water crevices before being able to reach a closed state. However, experimental evidence contradicts this observation, since the *Shaker* K^+ channel in the closed state may still carry solvated ions in its pore cavity [131–133]. Furthermore, inactivated ionic channels also contain water-filled crevices in their closed pores [123,124,134].

There are different approaches to simulate the application of an external electric field over the membrane akin to nsPEF protocols while running MD protocols. The most common one is introducing a uniform electric field $\vec{E}$ perpendicular to the membrane plane throughout the entire simulation box. This gives rise to a force $\vec{F} = q_i\vec{E}$ that is applied to all charges q_i in the simulation. The value of the transmembrane voltage (TMV) will be $\Delta V_m = EL_Z$, where L_Z is the length of the Z-axis of the simulation Box. In order to avoid the accumulation of ions when the external electric field is applied, it is recommended that this method be used in the absence of salts. It is important to address that this electric field implementation has a certain appearance of artificiality that can cause some concerns [135,136], mainly because the force over charged atoms is independent of their position.

A more realistic way to reproduce the TMV is through the method of imbalancing ions. In fact, the in vivo TMV is caused by a small charge imbalance across the membrane [137,138]. To mimic this imbalance, there are two different implementations. The first one, known as the two-membranes setup, is achieved by using a twin phospholipid bilayer system that includes two independent bulk phases with unequal ion distributions [135]. Despite being suitable to produce a TMV as a consequence of the ion imbalance, this

protocol significantly increases the number of atoms required for an MD simulation, scaling up the computational cost of the simulation. To bypass this problem, a second implementation was proposed, consisting of a single bilayer and an air–solvent interface, that also results in two independent bulk phases [136]. Despite being more efficient than the double-membrane method, this protocol may produce unwanted surface phenomena at the air–solvent interface.

5.3. Voltage-Gated Calcium Channel

Most of the available evidence suggests that the increase of cytoplasmic Ca^{2+} concentration is the result of nanopore formation at the cytoplasmic membrane. Back in 2002, Beebe et al. were the first to propose that ion channels could be possible targets of nsPEFs protocols [139]. Since that time, ion channels have gained protagonism in the field due to strong experimental evidence (see below). Intuitively, due to their sensitivity to changes in transmembrane potential and due to their ability to transport Ca^{2+}, the main target of nsPEF protocols should be Voltage-Gated Calcium Channels (VGCC).

VGCCs fall into two major categories: high-voltage-activated (HVA) channels that open in response to large changes in voltage across the cell membrane, and low-voltage-activated (LVA) channels, which are activated by small voltage changes [140,141] close to the typical resting membrane potential of neurons (∼80 mV). Based on biochemical and molecular analyses [142], HVA channels have been characterized as heteromultimeric protein complexes formed through the co-assembly of a pore-forming α_1 subunit, having ancillary $\alpha_2\gamma$, β, and γ subunits, whereas LVA channels appear to lack the latter. The α_1 subunit is the key determinant of calcium channel subtypes. There are three major families of α_1 subunits (termed Ca_v1, Ca_v2, and Ca_v3), each consisting of several members [143]. The Ca_v1 channel family encodes three different neuronal L-type channels (termed $Ca_v1.2$, $Ca_v1.3$, and $Ca_v1.4$) plus a skeletal-muscle-specific isoform, $Ca_v1.1$ [144–147]. These channels are sensitive to a number of different dihydropyridine (DHP) antagonists and agonists [148]. The Ca_v2 channel family includes three members ($Ca_v2.1$, $Ca_v2.2$, and $Ca_v2.3$). Through alternative splicing and assembly with specific ancillary subunits, $Ca_v2.1$ gives rise to P- and Q-type channels [149,150], which are both blocked (albeit with different affinities) by ω–agatoxin IVA, a peptide isolated from spider venom [151]. $Ca_v2.2$ encodes N-type channels [147,152] that are selectively inhibited by ω–conotoxins and the GVIA and MVIIA toxins isolated from mollusk venom. $Ca_v2.3$ corresponds to R-type channels [153] that can be inhibited by SNX-482, a peptide present in tarantula venom [154,155]. There are three types of Ca_v3 channels ($Ca_v3.1$, $Ca_v3.2$, and $Ca_v3.3$), all of which represent T-type calcium channels [156–158]. Ca_v3 channels can be distinguished by their sensitivity to nickel and relative resistance to blocking by cadmium ions, which block all HVA channels in the low micromolar range (for review, see [159]).

All ten α subunits share a common topology of four major transmembrane domains, each of them containing six membrane-spanning helices, termed S1 to S6. Helices S1 to S4 form the VSD, including the positively charged S4 segment, the key that controls voltage-dependent activation [160]. In addition, they have a typical re-entrant P loop motif between S5 and S6 that forms the permeation pathway (Figure 4). Each of the P loop regions contains highly conserved negatively charged amino acid residues (glutamate in HVA channels) that cooperate to form a pore that is highly selective for permeable cations such as calcium [161–163], barium, and strontium [164] and that interact with non-permeable divalent cations such as cadmium [165].

The majority of the structural/functional information about VGCC has been deduced from site-directed mutagenesis and generation of chimeric calcium channel subunits. Unlike potassium and bacterial sodium channels, it has not yet been possible to obtain crystallographic structural information concerning entire mammalian VGCC subunits, although structures of the $\alpha_2\gamma$ subunit bound to a fragment of the α_1 subunit I-II linker have been resolved by multiple groups [166,167]. Furthermore, co-crystallographic studies and even NMR structures of calmodulin bound to $Ca_v1.2$ and $Ca_v2.1$ have been re-

ported [168–174]. Cryo-EM structures have revealed crude structural information about this channel subtype [175–178]; however, they do not have enough resolution to gain insight into the structural basis of channel function. Based on the crystallographic structures of potassium channels released in 2005 [179], several homology models of α subunits have been constructed and used to model drug interactions, in particular with L-type channels [180–182]. While these works have provided some advances in our understanding of subunit regulation of VGCC, it remains to be determined whether the observed interactions are relevant to actual conformations in holochannels or perhaps modified by the presence of transmembrane regions and other intracellular domains. These studies about VGCC using the structures of other ion channels are supported by the fact that the fourth VSD subunit is ubiquitous to VGC [183] since the main differences in selectivity arise from the S6 transmembrane helix that forms the pore domain.

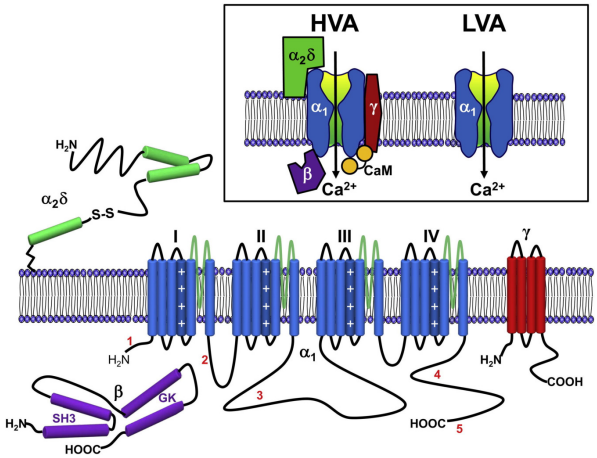

Figure 4. Representation of the membrane topology and secondary structure of HVA channels. In blue: the common structure of HVA and LVA channels, with their four VSD (I, II, III, and IV). The dark blue cylinder in each VSD is the charged S4 helix. The single blue cylinder in each VSD is the S6 helix that forms the pore domain. In green, purple, and red: the other subunits of HVA channel. The lengths of lines correspond approximately to the lengths of the polypeptide segments represented. Inbox at top: comparative representation of the structure of HVA and LVA calcium channels (α_1) and the subunits of HVA channels ($\alpha_2\delta$, β, and γ). Taken from the journal *Neuron*, article "Neuronal Voltage-Gated Calcium Channels: Structure, Function, and Dysfunction" [184].

Now that we have explored the topology, structure, and function of VGCC, we will focus on the literature suggesting that the application of nsPEF protocols may induce the activation of these channels. Rogers et al. in 2004 were the first group to stimulate isolated muscle fibers with an nsPEF (~1 ns, 24 kV/cm). They observed muscle contraction induced by the application of the nsPEF protocol and that the duration of the strength curve extended linearly up to 1 ns. According to these authors, these data suggest the activation of some ionic channel without electroporation. Moreover, they suggested that the most probable cause should be the increase of intracellular Ca^{2+} concentration via VGCC activation [185]. Later on in 2010, Craviso et al. used bovine cromaffin cells to apply an nsPEF protocol consisting of 50 kV/cm with a pulse cycle of 5 ns to show that the entry of Ca^{2+} is mainly through L-type VGCC. Consistently, ω–conotoxin GVIA (N-type VGCC blocker), ω–agatoxin IVA (P/Q-type VGCC blocker), and ω–conotoxin MVIIC (N/P/Q-type VGCC blocker) reduced the increase in cytoplasmic Ca^{2+}. Moreover, the simultaneous blockage of L-, N-, and P/Q-type channels by using a cocktail of VGCC inhibitors completely abolished Ca^{2+} entry. These results suggest that the increase in cytoplasmic Ca^{2+} occurs only through VGCC [186]. More recently, by using the human glioblastoma U87 MG cell line, Burke et al. demonstrated the role of VGCC, both L and T-type, in Ca^{2+} influx due to nsPEFs. On top of that, these authors also suggested that other ionic channels could be involved, such as the Ca^{2+}-gated BK potassium channel and

the TRPM8 (transient receptor potential) channel [187]. It is worth mentioning that Ca^{2+} channels were not uniquely identified as a target of the application of nsPEF protocols. Another ion channel more recently described as a nsPEF target is the Na^{+} voltage-gated channel (VGNC) [186,188]. These findings are of particular interest for the manipulation of excitable cells through nsPEF protocols: they can trigger action potentials in excitable cells by the activation of this channel. Thus, findings relating VGNC activation by nsPEF are exciting and deserve more attention. Table 2 was prepared to summarize the latest findings related to VGC activation by the application of nsPEF protocols, including VGNCs.

Table 2. Examples of studies demonstrating effects of nsPEF on VGCs.

nsPEF (kV/cm)	Pulse Time (ns)	Cell Line or Tissue Used	Observed Effect of nsPEF	Year and Citation
3.1	150–400	Bovine chromaffin cells	Similar results to [186]. Bagalkot et al. in 2019 incorporated a symmetrical bipolar pulse (a second identical pulse but with opposite polarity) that attenuated Ca^{2+} entry across possible nanopores while preserving Ca^{2+} influx through VGCCs [189].	2018 [189,190]
190	0.5	GH3, CHO-K1, and NG108 cells (murine neuroblastoma–rat glioma hybrid)	This sub-nanosecond electric pulse activated VGCCs on GH3 and NG108 cells (which express multiple types of VGCCs) and CHO-K1 cells (no VGCC expression). Trains of up to 100 pulses did not change the cytoplasmic Ca^{2+} concentration (followed by Fura-2 imaging) in CHO-K1 cells, while in GH3 and NG108, a single pulse significantly increased it. Trains of 100 pulses increased cytoplasmic Ca^{2+} concentration to 379 ± 33 nM in GH3 and 719 ± 315 nM in NG108. To corroborate that Ca^{2+} is passing through a VGCC and not nanopores, they used verapamil (L-type VGCC blocker) and ω–conotoxin (wide-spectrum N, P, and Q type VGCC blocker). They observed 80-100% inhibition of Ca^{2+} uptake with both VGCC blockers.	2015 [34]
2.3	300	HEK293 cells	In cells with and without assembled $Ca_v1.3$ L-type VGCC, the nsPEF pulse caused a lasting (>80 s) increase in membrane conductance for all cells. Although the elicited membrane potential did not depolarize enough for VGCC activation, the increase in conductance in cells that expressed VGCC was about two-fold greater than in cells which did not. This result suggests an important role of VGCC in the increase in cytoplasmic Ca^{2+} concentration induced by nsPEF.	2018 [191]
1.6–1.9	200	E18 rat hippocampal neurons	Using fast optical membrane potential imaging, it was shown that a single nsPEF pulse was able to trigger a single action potential 4–6 ms after the nsPEF pulse in 40% of neurons. The addition of tetrodotoxin (selective sodium channel blocker) to cell media abolished the induced nsPEF action potential, demonstrating that nsPEF managed to activate VGNCs.	2017 [188]
3.3–8.8	12	*Xenopus laevis* peripheral nerve	Using thousands of nsPEF pulses, nerve excitation was achieved without electroporation for the first time. The nerves did not register cumulative damage, as refractory properties were not affected. The authors claimed that their data proved that VGNC are activated by nsPEFs and also manifested that nsPEFs are a promising tool for biomedical applications.	2010 [186]

6. Protein-Mediated Electroporation: An Additional nsPEF Effect?

As discussed above, there is plenty of evidence supporting the notion that lipidic nanopores are formed in the internal cellular membranes due to the application of an nsPEF protocol. Moreover, theoretical approaches also support this notion, leading to the conclusion that some electroporation protocols may change the permeability of cellular organelles [192]. Therefore, the definition of electroporation should be extended to include transient changes in the semi-permeability of both cytoplasmic and internal membranes. It is well known that the transient loss of semi-permeability of cellular membranes by an external electric stimulus is not only due to the formation of aqueous lipidic pores but may also occur by a broader range of biophysical and biochemical mechanisms, ranging from pH changes, the use of chaotropic agents, and ion imbalance [193]. For this reason, the term *electropermeabilization* has being coined in the field to refer to changes in membrane permeabilization, not necessarily due to the formation of lipidic pores. By contrast, the term electroporation should strictly be used to refer to changes in the membrane solely as a result of the formation of aqueous lipidic pores [193]. As a consequence, we will discuss additional electropermeabilization processes that may occur due to the application of nsPEF protocols. To do so, we will focus on the role of transmembrane proteins other than ion channels (discussed in Section 5). The first association between transmembrane proteins and electropermeabilization processes occurred in 1980: the application of an external electric stimulus in erythrocytes produced an incremental increase in the electrical

conductivity of the transmembrane Na^+/K^+-ATPases [194]. Ten years had to pass for a scientifically sound explanation of this phenomenon: the external electrical stimuli would generate sufficient heat over the protein for its denaturation, permitting the passage of ions, generating the measured macroscopic current [4,195].

The application of MD protocols has further expanded the mechanistic comprehension of the electropermeabilization process that could be mediated by transmembrane proteins. Recent evidence coming from the application of external stimuli mimicking the application of nsPEF in MD simulations points towards the formation of pores in transmembrane proteins. The first work studying pore formation in transmembrane proteins by the application of an electric stimulus using MD simulation was published in 2018 [196]. In this study, an intraprotein electropore persisting more than ~50 ns was produced in a human aquaporin when the simulation box was subjected to a continuous electric field of 0.2 V/nm. Of note, this electropore was resealed within ~20 ns after turning off the external electric field. By performing an MD protocol, Rems et al. (2020) [197] registered the formation of either simple or complex pores located in the VSD in three distinct VGCs: a bacterial VGNC, a eukaryotic VGNC, and a human hyperpolarization-activated cyclic nucleotide-gated channel. Complex pores are produced by massive rearrangements of transmembrane segments of the affected channels and have been proposed as the source of the theorized lipidic pores that may be stabilized by the presence of ions and other parts of the channels, such as TMHs [198–200]. When the three aforementioned VGCs are subjected to an oscillating hyperpolarizing/depolarizing TMV of ±1.5 V for 600 ns, the formation of different protein pores is promoted. Interestingly, Rems et al. discuss that the formation of simple and complex pores at the VSD can explain some experimental observations: (i) major VSD rearrangements are expected to turn the VSD dysfunctional, disrupting the gating of VGCs. This phenomenon could explain electrophysiological measurements showing that electroporative submicrosecond electric pulses can decrease ionic currents through VGNC and VGCC channels in different excitable cells [201–203]; (ii) some VSDs are easier to be porated than others, which may explain why some channels appear to be affected at weaker electric fields than others [203]; (iii) structurally different pores forming in the VSDs at either hyperpolarizing or depolarizing TMV may explain why the decrease in channel conductance depends on the polarity of the TMV [204]; (iv) observed complex pores remained open during a 1 μs simulation, suggesting that, at least during that timeframe, the VSD would not spontaneously refold back. These complex pores observed in MD simulation, lasting from tens to hundreds of nanoseconds [205,206], offer an interesting point of view to the discussion of why cell membranes remain permeable for seconds or minutes after application of nsPEF protocols [193].

Recently, our group published an MD simulation article in which we also observed the formation of complex pores in a VSD, in this case belonging to a human VGCC [207]. These pores were created by the application of an external electric field of 0.2 V/nm for 50 ns (mimicking an nsPEF) using a cellular membrane prototype containing POPC and cholesterol in a 1:3 ratio. Reformulating the topic of this section as the capability of nsPEF to induce pores in transmembrane proteins, we may argue that in the available literature there is robust data obtained from MD simulations supporting a positive answer. However, to fully address this question, experimental data are mandatory. We strongly support Rems et al. [197] exhortation to experimentalists for further investigation in this issue. We certainly agree that eventual biotechnological applications for such an nsPEF device capable of forming protein pores are highly stimulating to the imagination. For further insights on the role of MD simulations to study the effects of nsPEF protocols, in particular conformational changes occurring on the kinesin nanomotor and other proteins, please refer to [208,209], respectively.

7. nsPEF Applications

In the following section, we briefly review some applications of nsPEF technology. Despite still being under development, there are interesting perspectives regarding the

development of standard nsPEF devices that may be widely used in the near future, particulary in health-related applications. As mentioned before, nsPEF is a versatile, non-invasive, and cheap technology that can manipulate cellular membranes and even transmembrane proteins with an exquisite fine-tuning.

7.1. In Human Health

- **Activation of excitable cells**:

  Cardiac cells: nsPEF (10–80 kV/cm, 4 ns, 1–20 pulses with 200/400/600 ms intervals) can indirectly lead to cardiac cell excitation. Of note, these results challenge the concept of chronaxie: minimum time required for an electric current to double the strength of the rheobase in order to stimulate a muscle or a neuron. The use of nsPEF technology to excite cardiac cells and mobilize intracellular Ca^{2+} may prove valuable for cardiac pacing and defibrillation [210]. For other related studies see [211–213].

  Neurons: nsPEF (27.8 kV/cm, 10 ns, single pulse) was sufficient to initiate action potentials. The observed effect was repeatable and stable. These results highlight the potential use of ultrashort pulsed electric fields for stimulation of subcortical structures and suggest they may be used as a wireless alternative for deep brain stimulation [214]. For other related studies see [188,215–217].
- **Phenotype manipulation**:

  Differentiation: nsPEF (1.5–25 kV/cm, 300 ns, 5 pulses) can induce proliferation and myotubule maturation or nodule formation in myoblasts and osteoblasts, respectively. Myoblasts were isolated from hind-limb skeletal muscle of four-week-old mice $Pten^{MKO}$, and primary human osteoblasts were obtained from a vendor (Sciencell®) [218].

  Dedifferentiation: nsPEF (10–20 kV/cm, 100 ns pulse) induces dedifferentiation partially through transient activation of the wnt/β–catenin signaling pathway in porcine chondrocytes [219].
- **Gene expression**: nsPEF (20 kVcm, 80 ns, various combinations of pulses) dramatically elevated c-Jun and c-Fos mRNA levels, which correlated with the observation of c-Jun N-terminal kinase (JNK) pathway activation in HeLa S3 [220]. For related studies see [219,221–224].
- **ntiparasitic**: Cystic echinococcosis is a widely endemic helminthic disease caused by infection with metacestodes (larval stage) of the *Echinococcus granulosus* tapeworm. Application of nsPEF (21 KV/cm, 300 ns, 100 pulses) caused a significant increase in the death rate of protoscolices (future heads of the adult worms) [225]. For related studies see [226,227].
- **Wound healing**: nsPEF (30 kV/cm, 300 ns) induced platelet rich plasma aggregation and platelet gel formation. These gels are applied to soft and hard tissue wounds, where they enhance healing [30]. For other related studies see [228–230].
- **Immune response**: Using in vivo experiments, nsPEF (15 kV, 100 ns, 400 pulses) induced translocation of calreticulin in rat tumor cell-surfaces, a molecular pattern associated with damage that is indicative of immunogenic cell death (ICD). The nsPEF also triggered CD8-dependent inhibition of secondary tumor growth, concluded by comparing the tumor size using rats depleted of $CD8^+$ cytotoxic T-cells under the same nsPEF treatment. The first group showed an average size of only 3% of the primary tumor size compared with the 54% shown by the $CD8^+$-depleted rats. Additionally, with immunohistochemistry it was observed that $CD8^+$ T-cells were highly enriched in the first group. Furthermore, it was shown that vaccinating rats with isogenic tumor cells (MCA205 fibrosarcoma cell line) treated with nsPEF (50 kV, 100 ns, 500 pulses) stimulates an immune response that inhibits the growth of secondary tumors in a $CD8^+$-dependent manner [231]. This work opens the door to the fabrication of cell-based vaccines using nsPEF stimulation to promote an improved immune response. For other related studies reporting tumor ablation through an antitumor immune response using nsPEF see [232–236].

- **Cancer**: This is by far the most-studied nsPEF application, with 46 in vitro studies up to 2016 [27] and over 100 so far. Recently, preclinical animal studies have demonstrated that nsPEF can induce local and systemic $CD8^+$ T-cell mediated adaptive immune response against tumors [233,236]. In clinical trials, nsPEF proved to be a safe and effective therapy against basal cell carcinoma [237,238]. There are other novel techniques to combat cancer that also use electric fields, known as electrochemotherapy [239,240], irreversible electroporation [7], and electro-gene therapy [7]. Electrochemotherapy and electro-gene therapy use electroporation to achieve the anti-tumoral effect of other agents. In irreversible electroporation, cytoplasmic membranes of tumor cells cannot recover from permeabilization, causing cell death mainly by necrosis. Unlike the just mentioned electro-technique, nsPEF is cell-dependent. A possible explanation for this may be related to apoptosis (programmed cell death type 1 [241]), which is a tightly controlled cell process and different in each cell type [242]. Thus, if nsPEF induces apoptosis, as seems to be the case, it is expected to exhibit cell-dependent responses. This makes nsPEF an extraordinary tool, with specific responses based on tuning the intensity, duration, and number of pulses. There are several examples of cell dependence and nsPEF. Stacey et al. in 2002 demonstrated that exposing cancer cells to nsPEF with 60 kV/cm could induce DNA damage [243] (Figure 5). Beebe et al. in 2002 studied the antitumor effects of nsPEF on Jurkat cells, with pulses at 60, 150, and 300 kV/cm [139]. Xinh ua Chen et al. in 2012 applied nsPEF with 900 pulses at 68 kV/cm to ablate hepatocellular carcinoma [244]. Nuccitelli et al. in 2013 inhibited human pancreatic carcinoma using 100 pulses of 100 ns duration and 30 kV/cm [245]. More importantly for nsPEF as cancer treatment, tumor cells are more sensitive to nsPEF than normal cells [246]. See Figure 6 for an example of a nsPEF device suitable for use in cancer treatment.

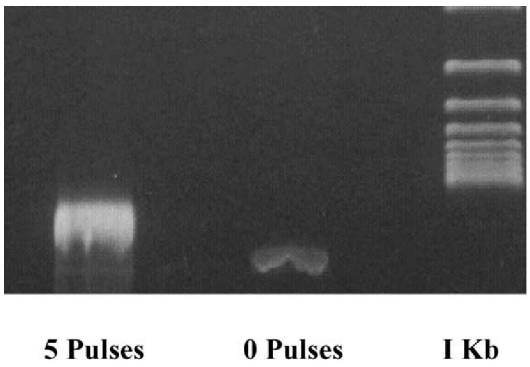

Figure 5. Electrophoresis of DNA extracted from Jurkat cells right after nsPEF (60 kV/cm, 60 ns, 5 pulses). The appearance of a smeared DNA band in the first lane is congruent with DNA damage induced by nsPEF. Taken from [247]. Reproduced with permission.

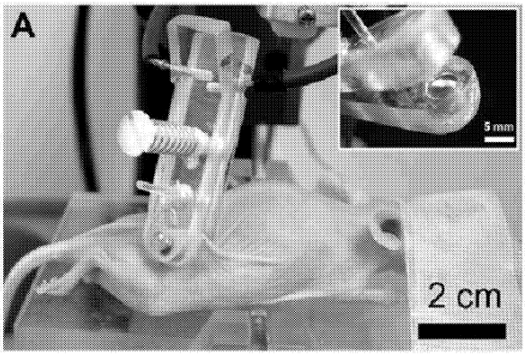

Figure 6. nsPEF device applied on SKH-1 hairless mouse to abolish melanoma cancer. Figure extracted from the patent titled "Nanosecond pulsed electric fields cause melanomas to self-destruct". ID US20180200510A1.

7.2. Industrial

- **Cell proliferation**: nsPEF (10 kV/cm, 100 ns) can increase *Arthrospira platensis* SAG 21.99 (a cyanobacteria) cell growth after repeated pulses in the exponential growth phase. The effect was most pronounced five days after treatment. Treatments with nsPEF might improve sustainable and economical microalgae-based biorefineries [24]. For other studies see [218,248,249].
- **Fermentation industry**: nsPEF (15 kV/cm, 100 ns, 20 pulse) increased avermectin (anthelmintic and insecticidal agent) production in *Streptomyces avermitilis* by 42% and reduced the time needed for reaching a plateau in the fermentation process from 5 to 7 days [250]. For other related studies see [251].
- **Food industry**: Microalgae are a novel food ingredient of increasing interest as they can be grown on non-arable lands and fixates CO_2 when grown photoautotrophically. Treatment with nsPEF (5–100 kV/cm, 2–100 ns) reduced total bacterial contamination $>\log_{10}$ in *Chlorella vulgaris* cultures without compromising the microalgae. For related studies see [252,253].
- **Seed germination**: nsPEF (10–30 kV/cm, 100 ns, 20 pulses) application significantly affected seed germination and pre-growth of *Haloxylon ammodendron* (Figure 7). This is probably due to the exogenous and endogenous NO generated in the nsPEF seed-treatment system [254]. For related studies see [255,256].

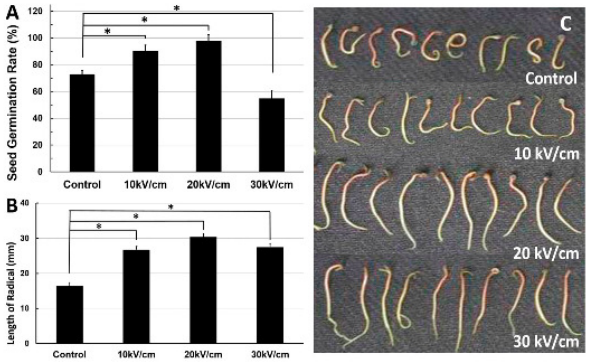

Figure 7. Effects of different intensities of nsPEF on the seed germination rate and radical length of *Haloxylon ammodendron*. (**A**): Seed germination rate at different electric fields. (**B**): Length of radical at different electric fields. (**C**): Image of radical length at different electric fields. Taken from the journal *Plasma Processes and Polymers*, article "Early Growth Effects of Nanosecond Pulsed Electric Field (nsPEFs) Exposure on *Haloxylon ammodendron*". Copyright Wiley–VCH GmbH. Reproduced with permission.

8. Challenges and Future Perspectives of nsPEF's Effect on Cells

As a relatively new technology (just 25 years old), the accelerated development of nsPEF comes with a series of challenges. While some are the lack of experimental setups to follow changes in membranes at the nanosecond time scale, others are related to the lack of experimental evidence supporting the formation of nanopores in proteins. On top of these, the existence of contradictory results related to both the temporal scale and the actual target (as discussed in previous sections) are a matter of active debate in the community. However, being the first drug-free, non-ionizing technology directly affecting cellular organelles, nsPEF opens a biotechnological Pandora's box potentially enabling exciting new applications in a variety of fields. Therefore, a compendium of both experimental and theoretical data are needed in order to promote a better understanding of this extraordinary phenomenon. Focusing on this aim, in the following section we offer a brief discussion of some other relevant topics surrounding this amazing technology.

8.1. Nomenclature, Abbreviations, and Mathematical Formulas

While some authors refer to this technology as "Nanopulse Stimulation (NPS)", others may use "Nanosecond Pulsed Electric Field (nsPEF)". Thus, using only one of these nomenclatures and/or abbreviations while searching the literature may lead to missing some valuable research. It is worth mentioning that nsPEF seems to be a much better term than NPS because the latter is widely used in other fields to refer to: nanoparticles (NPs) in nanotechnology [257,258]; noise-power spectrum (NPS) in electronics and signal analysis [259,260]; and net promoter score (NPS) in economics and customer care [261,262].

A brief but important mathematical formalism: the parameter τ_m may lead to some confusion (see Section 4). This symbol represents the membrane relaxation time-constant (for cytoplasmic or internal membranes) and not the charging time of the membrane. Keeping this difference in mind is important because their confusion may affect the outcome of experimental protocols. For instance, to produce an effect on internal membranes rather than the cytoplasmic membrane, a pulse duration below the membrane charging time should be used. It is important to remark that to achieve 95% of the charging capacity of the membrane, $\sim 3\tau_m$ time should be elapsed. Therefore, in order to affect mainly the internal membranes, a pulse duration below $\sim 3\tau_m$ should be used.

It has also been recommended by several authors not to assume that every cell line has a τ_m near 100 ns, as is described in some articles as an approximate value of τ_m for mammalian cells. Theoretical approaches postulate that τ_m is directly proportional to the cell radius and has a strong dependency on the cytoplasmic conductivity and cell medium conductivity (Equation (3)). Thus, τ_m is a cell-dependent value not only influenced by the size but also by the inner ionic strength and that can be modulated by changing the medium conductivity. Taking all of this information into account, when choosing an nsPEF protocol to accomplish a desired cell effect, it is highly recommended to consider cell size, membrane composition, and medium conductivity.

8.2. Nanopores

As mentioned before, there is a lack of experimental evidence demonstrating the formation of nanopores. However, theoretical data, mainly coming from MD simulations, and indirect experimental evidence suggest the formation of these structures as a primary nsPEF effect. Nevertheless, as discussed in Section 3, their exact localization, either on the cytoplasmic membrane or internal membranes, is still a matter of debate. The actual capability of internal membranes to be perturbed by an external electric field due to the application of nsPEF depends, as discussed in Section 4, mainly on the time and intensity of exposure. If the exposition time is larger than that of the charging time of the cytoplasmic membrane, then the electric field in the interior of the cell will be nullified (Figure 3) and any nanopore formation should be neglected in the internal membranes. That being said, many of the analyses of classic articles in the field speculate precipitation effects. It is expected that during the application of nsPEF, before the cytoplasmic membrane charge time is achieved, the cell interior is actually exposed to the electric field. Hence, an inner ionic current could be induced by the movement of charges, making the membrane voltage difference large enough to induce nanopore formation in internal membranes. These internal nanopores could play an important role to better explain the nsPEF effect, particularly when contrasted with the classic view allowing the formation of nanopores exclusively on the cytoplasmic membrane. Of note, the internal nanopore hypothesis is supported by evidence pointing towards the lifetime of nanopores varying from nanoseconds up to 1 s, according to early results [35,45,95,263–265]. Moreover, recent results increase the duration of nanopores even to the order of minutes, a timeframe where cells exposed to cytoplasmic membrane pores will collapse due to osmotic shock or will undergo apoptosis or necrosis depending on the cellular pathways activated [3,52,53,266–269].

Nanopores, Cholesterol, and Cancer

A player largely omitted in the study of nsPEF's effect on cells is cholesterol. This molecule is of vital importance to membrane physicochemical properties, but scarce knowledge relates the effect of cholesterol concentration with the formation of nanopores due to the application of nsPEF protocols. Moreover, the abundant evidence described on Section 3 strongly supports the inclusion of cholesterol in future studies for a better comprehension of its role during the application of nsPEF protocols. This will be, in fact, important knowledge considering different cell types exhibit a variety of cholesterol concentrations in their membranes. In particular, further studies should pay attention to understanding how cholesterol changes important physicochemical properties of membranes. When a pore membrane is formed, phospholipids migrate to the pore center in order to hide their hydrophobic carbon chains, exposing their polar groups to the solvent in order to equilibrate the forming pore [270]. Despite being a spontaneous process, the reorganization of phospholipids has an energetic cost associated with the breaking of van der Waals forces between carbon aliphatic chains participating in this rearrangement. This energy penalty per unit length of pore circumference is known as edge tension and denotes a driving force tending to close transient pores [271]. Edge tension is closely related to two important parameters guiding nanopore formation: (i) the membrane charge necessary to induce the nanopore, which is related to nsPEF intensity and duration; and (ii) the lifetime of nsPEF nanopores, which is related to the auto-healing capacity of lipid bilayer structures. Therefore, measuring edge tension is important not only for nsPEF research, but also to better understand various biological events and physicochemical processes occurring in membranes. Of note, MD simulation studies have being used to propose edge tension values [272,273].

As seen in the previous paragraph, the concentration of cholesterol has a strong impact on the edge tension of cellular membranes. Therefore, the presence of cholesterol should also have important consequences for the modulation of nsPEF's effects in cells. Consistently, cholesterol content together with the phospholipid profile have both been proposed as important factors to explain nsPEF selectivity for different cell types [274]. Of note, available literature suggests that various solid tumors and malignancies present a dysregulated cholesterol metabolism, a characteristic that may be related to the high sensitivity of these cells to the application of nsPEF protocols [275]. Thus, the phospholipid profile in different cancer cell lines is notoriously altered when compared with their non-cancerous counterparts—an important prognosis of cancer malignancy [276–280]. Interestingly enough, the presence of lipid rafts, i.e., membrane domains rich in cholesterol, is also scarcely explored with regard to its relationship to nsPEF's effects. Abundant literature suggests that the presence of lipid rafts is crucial to anchor ion channels and other transmembrane proteins [281,282]. On top of that, the increased amount of phospholipids in cancer cells occurs mainly on regions forming lipid rafts [280,283]. Even more, the dysregulation of lipid rafts occurring in cancer promotes cell transformation, tumor progression, and metastasis [280]. Considering the available evidence, dissecting the role of cholesterol and phospholipid profiles during the application of nsPEF protocols could be crucial to better understand the sensitivity of cancer cells to this technology—a necessary step towards the development of novel nsPEF-based cancer therapies.

9. Conclusions

Despite the controversy in the academic community arising from the timescale in which nsPEF effects are elicited, the key effect at the cellular level is, undoubtedly, the change in Ca^{2+} homeostasis. Whether this change is due to the formation of membrane nanopores either on the plasma membrane or internal membranes is still a matter of debate and probably dependent on the parameters of the applied protocols. On top of that, abundant evidence supports the notion that the formation of membrane nanopores is linked to the activation of VG channels. Moreover, recently published data coming from MD simulations show that the application of nsPEF-like protocols may also form transient pores within

the structure of VGC channels. As a whole, both cell membranes and ion channels should be considered as equally relevant contributors to explain the effects of the application of nsPEF protocols.

In spite of the impressive and massive advancements supporting the development of nsPEF technology, a larger body of research is still needed to better understand the fundamental biophysical principles governing the effects of nsPEF. A better understanding of this interesting phenomenon will eventually allow its translation into a broader and more robust set of applications. To this end, both public and private parties have to become aware of the exceptional capabilities of nsPEF technology and its suitability to be used in both industry and human health.

Author Contributions: Conceptualization, investigation, writing the original review, A.R.R.-F.; investigation, writing the original review, L.C.; visualization, data curation, S.E.G.-M.; visualization, data curation, G.N.; writing, review and editing, F.V.; review, editing, project administration, funding acquisition, T.P.-A. All authors have read and agreed to the published version of the manuscript.

Funding: The authors are pleased to acknowledge financial support from FONDECYT Iniciación 11221268, Fondecyt Postdoctorado 3200937 and from Centro Ciencia & Vida, FB210008, Programa de Financiamiento Basal para Centros Científicos y Tecnológicos de Excelencia de ANID.

Institutional Review Board Statement: Not applicable.

Informed Consent Statement: Not applicable.

Data Availability Statement: Not applicable.

Acknowledgments: The authors are especially grateful to Beebe and Schoenbach, pioneers of nsPEF studies, for their useful comments to improve this contribution. The authors also give thanks to the journal *Plasma Processes and Polymers* and to the journal *Mutation Research/Genetic Toxicology and Environmental Mutagenesis* for their permission to include Figures 5 and 7, respectively.

Conflicts of Interest: The authors declare no conflict of interest. The funders had no role in the design of the study; in the collection, analyses, or interpretation of data; in the writing of the manuscript, or in the decision to publish the results.

Abbreviations

The following abbreviations are used in this manuscript:

nsPEF	Nanosecond Pulsed Electric Field
NPS	Nano Pulsed Stimulation
IRA	impulse radiating antenna
CaBP	calcium-binding proteins
POPC	1-palmitoyl-2-oleoyl-sn-glycero-3-phosphocholine
$\vec{E}$	electric field
$\vec{F}$	force
ΔV	voltage difference
d	membrane thickness
q	charge
MD	Molecular Dynamics
MβCD	methyl-β-cyclodextrin
MTT	3-(4,5-dimethylthiazol-2-yl)-2,5-diphenyl tetrazolium bromide
τ	time-constant
R	resistance
C	capacitance
t	time
$V(t)$	voltage at certain time t
$V_g(t)$	voltage difference across the cytoplasmatic membrane
a	cell radius
θ	polar angle

τ_m	membrane relaxation time-constant
C_m	membrane capacitance
σ_e	external conductivity
σ_i	internal conductivity
VGC	Voltage-Gated Channels
VSD	Voltage Sensing Domain
FRET	fluorescent resonance energy transfer
ΔV_m	membrane voltage difference
L_Z	length of the Z-axis of the simulation Box
TMV	transmembrane voltage
VGCC	Voltage-Gated Calcium Channels
HVA	high-voltage-activated HVA
LVA	low-voltage-activated
DHP	dihydropyridine
VGNC	Na^+ voltage-gated channel

References

1. Meijerink, M.R.; Scheffer, H.J.; Narayanan, G. *Irreversible Electroporation in Clinical Practice*; Springer: Berlin/Heidelberg, Germany, 2018.
2. Neumann, E.; Schaefer-Ridder, M.; Wang, Y.; Hofschneider, P. Gene transfer into mouse lyoma cells by electroporation in high electric fields. *EMBO J.* **1982**, *1*, 841–845. [CrossRef] [PubMed]
3. Pakhomov, A.G.; Bowman, A.M.; Ibey, B.L.; Andre, F.M.; Pakhomova, O.N.; Schoenbach, K.H. Lipid nanopores can form a stable, ion channel-like conduction pathway in cell membrane. *Biochem. Biophys. Res. Commun.* **2009**, *385*, 181–186. [CrossRef] [PubMed]
4. Tsong, T.Y. On electroporation of cell membranes and some related phenomena. *Bioelectrochem. Bioenerg.* **1990**, *24*, 271–295. [CrossRef]
5. Orlowski, S.; Belehradek, J., Jr.; Paoletti, C.; Mir, L.M. Transient electropermeabilization of cells in culture. Increase of the cytotoxicity of anticancer drugs. *Biochem. Pharmacol.* **1988**, *37*, 4727–4733. [CrossRef]
6. Miklavčič, D.; Mali, B.; Kos, B.; Heller, R.; Serša, G. Electrochemotherapy: From the drawing board into medical practice. *Biomed. Eng. Online* **2014**, *13*, 29. [CrossRef] [PubMed]
7. Davalos, R.V.; Mir, L.; Rubinsky, B. Tissue ablation with irreversible electroporation. *Ann. Biomed. Eng.* **2005**, *33*, 223. [CrossRef]
8. Yarmush, M.L.; Golberg, A.; Serša, G.; Kotnik, T.; Miklavčič, D. Electroporation-based technologies for medicine: Principles, applications, and challenges. *Annu. Rev. Biomed. Eng.* **2014**, *16*, 295–320. [CrossRef]
9. Kotnik, T.; Frey, W.; Sack, M.; Meglič, S.H.; Peterka, M.; Miklavčič, D. Electroporation-based applications in biotechnology. *Trends Biotechnol.* **2015**, *33*, 480–488. [CrossRef]
10. Mahnič-Kalamiza, S.; Vorobiev, E.; Miklavčič, D. Electroporation in food processing and biorefinery. *J. Membr. Biol.* **2014**, *247*, 1279–1304. [CrossRef]
11. Saldaña, G.; Álvarez, I.; Condón, S.; Raso, J. Microbiological aspects related to the feasibility of PEF technology for food pasteurization. *Crit. Rev. Food Sci. Nutr.* **2014**, *54*, 1415–1426. [CrossRef]
12. Schoenbach, K.H.; Alden, R.W.; Fox, T.J. Biofouling prevention with pulsed electric fields. In Proceedings of the 1996 International Power Modulator Symposium, Boca Raton, FL, USA, 25–27 June 1996; pp. 75–78.
13. Baum, C.E. Producing large transient electromagnetic fields in a small region: An electromagnetic implosion. In *Ultra-Wideband Short-Pulse Electromagnetics 8*; Springer: Berlin/Heidelberg, Germany, 2007; pp. 97–104.
14. Heeren, T.; Camp, J.T.; Kolb, J.F.; Schoenbach, K.H.; Katsuki, S.; Akiyama, H. 250 kV sub-nanosecond pulse generator with adjustable pulse-width. *IEEE Trans. Dielectr. Electr. Insul.* **2007**, *14*, 884–888. [CrossRef]
15. Plattner, H.; Verkhratsky, A. The ancient roots of calcium signalling evolutionary tree. *Cell Calcium* **2015**, *57*, 123–132. [CrossRef] [PubMed]
16. Kazmierczak, J.; Kempe, S.; Kremer, B. Calcium in the early evolution of living systems: A biohistorical approach. *Curr. Org. Chem.* **2013**, *17*, 1738–1750. [CrossRef]
17. Verkhratsky, A.; Burnstock, G. Biology of purinergic signalling: Its ancient evolutionary roots, its omnipresence and its multiple functional significance. *Bioessays* **2014**, *36*, 697–705. [CrossRef]
18. Haeseleer, F.; Sokal, I.; Verlinde, C.L.; Erdjument-Bromage, H.; Tempst, P.; Pronin, A.N.; Benovic, J.L.; Fariss, R.N.; Palczewski, K. Five members of a novel Ca^{2+}-binding protein (CABP) subfamily with similarity to calmodulin. *J. Biol. Chem.* **2000**, *275*, 1247–1260. [CrossRef]
19. Kinjo, T.G.; Schnetkamp, P.P. Ca^{2+} chemistry, storage and transport in biologic systems: An overview. In *Madame Curie Bioscience Database [Internet]*; Landes Bioscience: Austin, TX, USA, 2013.
20. Jaiswal, J. Calcium—How and why? *J. Biosci.* **2001**, *26*, 357–363. [CrossRef]
21. Williams, R.J. The evolution of calcium biochemistry. *Biochim. Biophys. Acta (BBA)-Mol. Cell Res.* **2006**, *1763*, 1139–1146. [CrossRef]
22. Morgan, R.; Martin-Almedina, S.; Iglesias, J.; Gonzalez-Florez, M.; Fernandez, M. Evolutionary perspective on annexin calcium-binding domains. *Biochim. Biophys. Acta (BBA)-Mol. Cell Res.* **2004**, *1742*, 133–140. [CrossRef]

23. Haynes, L.P.; McCue, H.V.; Burgoyne, R.D. Evolution and functional diversity of the Calcium Binding Proteins (CaBPs). *Front. Mol. Neurosci.* **2012**, *5*, 9. [CrossRef]
24. Buchmann, L.; Frey, W.; Gusbeth, C.; Ravaynia, P.S.; Mathys, A. Effect of nanosecond pulsed electric field treatment on cell proliferation of microalgae. *Bioresour. Technol.* **2019**, *271*, 402–408. [CrossRef]
25. Harburger, D.S.; Calderwood, D.A. Integrin signalling at a glance. *J. Cell Sci.* **2009**, *122*, 159–163. [CrossRef] [PubMed]
26. Zhu, J.K. Abiotic stress signaling and responses in plants. *Cell* **2016**, *167*, 313–324. [CrossRef] [PubMed]
27. Napotnik, T.B.; Reberšek, M.; Vernier, P.T.; Mali, B.; Miklavčič, D. Effects of high voltage nanosecond electric pulses on eukaryotic cells (in vitro): A systematic review. *Bioelectrochemistry* **2016**, *110*, 1–12. [CrossRef] [PubMed]
28. Beebe, S.J.; White, J.; Blackmore, P.F.; Deng, Y.; Somers, K.; Schoenbach, K.H. Diverse effects of nanosecond pulsed electric fields on cells and tissues. *DNA Cell Biol.* **2003**, *22*, 785–796. [CrossRef]
29. Thompson, G.L.; Roth, C.C.; Dalzell, D.R.; Kuipers, M.A.; Ibey, B.L. Calcium influx affects intracellular transport and membrane repair following nanosecond pulsed electric field exposure. *J. Biomed. Opt.* **2014**, *19*, 055005. [CrossRef]
30. Zhang, J.; Blackmore, P.F.; Hargrave, B.Y.; Xiao, S.; Beebe, S.J.; Schoenbach, K.H. Nanosecond pulse electric field (nanopulse): A novel non-ligand agonist for platelet activation. *Arch. Biochem. Biophys.* **2008**, *471*, 240–248. [CrossRef]
31. Beebe, S.J.; Fox, P.M.; Rec, L.J.; Willis, E.L.K.; Schoenbach, K.H. Nanosecond, high-intensity pulsed electric fields induce apoptosis in human cells. *FASEB J.* **2003**, *17*, 1493–1495. [CrossRef]
32. Semenov, I.; Xiao, S.; Pakhomov, A.G. Primary pathways of intracellular Ca^{2+} mobilization by nanosecond pulsed electric field. *Biochim. Biophys. Acta (BBA)-Biomembr.* **2013**, *1828*, 981–989. [CrossRef]
33. Vernier, P.T.; Ziegler, M.J.; Sun, Y.; Gundersen, M.A.; Tieleman, D.P. Nanopore-facilitated, voltage-driven phosphatidylserine translocation in lipid bilayers—In cells and in silico. *Phys. Biol.* **2006**, *3*, 233. [CrossRef]
34. Semenov, I.; Xiao, S.; Kang, D.; Schoenbach, K.H.; Pakhomov, A.G. Cell stimulation and calcium mobilization by picosecond electric pulses. *Bioelectrochemistry* **2015**, *105*, 65–71. [CrossRef]
35. Vernier, P.T.; Sun, Y.; Marcu, L.; Craft, C.M.; Gundersen, M.A. Nanoelectropulse-induced phosphatidylserine translocation. *Biophys. J.* **2004**, *86*, 4040–4048. [CrossRef] [PubMed]
36. Vernier, P.T.; Sun, Y.; Marcu, L.; Craft, C.M.; Gundersen, M.A. Nanosecond pulsed electric fields perturb membrane phospholipids in T lymphoblasts. *FEBS Lett.* **2004**, *572*, 103–108. [CrossRef] [PubMed]
37. Semenov, I.; Casciola, M.; Ibey, B.L.; Xiao, S.; Pakhomov, A.G. Electropermeabilization of cells by closely spaced paired nanosecond-range pulses. *Bioelectrochemistry* **2018**, *121*, 135–141. [CrossRef] [PubMed]
38. Semenov, I.; Xiao, S.; Pakhomova, O.N.; Pakhomov, A.G. Recruitment of the intracellular Ca^{2+} by ultrashort electric stimuli: The impact of pulse duration. *Cell Calcium* **2013**, *54*, 145–150. [CrossRef] [PubMed]
39. Ryan, H.; Zhou, C.; Gianulis, E.; Xiao, S. Non-Invasive nsPEF Stimulation for Biomodulation. Available online: https://www.researchgate.net/profile/Hollie-Ryan-2/publication/324223510_Non-Invasive_nsPEF_Stimulation_for_Biomodulation/links/5ac61c0fa6fdcc051db012fc/Non-Invasive-nsPEF-Stimulation-for-Biomodulation.pdf (accessed on 27 April 2022).
40. Beebe, S.J.; Chen, X.; Kolb, J.; Schoenbach, K.H. Non-ionizing radiation generated by nanosecond pulsed electric fields (nspefs) induce apoptosis in cancer in vivo. In Proceedings of the 2008 IEEE 35th International Conference on Plasma Science, Karlsruhe, Germany, 15–19 June 2008; p. 1.
41. Napotnik, T.B.; Wu, Y.H.; Gundersen, M.A.; Miklavčič, D.; Vernier, P.T. Nanosecond electric pulses cause mitochondrial membrane permeabilization in Jurkat cells. *Bioelectromagnetics* **2012**, *33*, 257–264. [CrossRef]
42. Beebe, S.J.; Sain, N.M.; Ren, W. Induction of cell death mechanisms and apoptosis by nanosecond pulsed electric fields (nsPEFs). *Cells* **2013**, *2*, 136–162. [CrossRef]
43. Hu, Q.; Joshi, R. Model evaluation of changes in electrorotation spectra of biological cells after nsPEF electroporation. *IEEE Trans. Dielectr. Electr. Insul.* **2010**, *17*, 1888–1894. [CrossRef]
44. Schoenbach, K. Bioelectric effect of intense nanosecond pulses. In *Advanced Electroporation Techniques in Biology and Medicine*; Pakhomov, A.G., Miklavcic, D., Markov, M.S., Eds.; CRC Press: Boca Raton, FL, USA, 2010.
45. Gowrishankar, T.; Weaver, J.C. Electrical behavior and pore accumulation in a multicellular model for conventional and supra-electroporation. *Biochem. Biophys. Res. Commun.* **2006**, *349*, 643–653. [CrossRef]
46. Kotnik, T.; Miklavčič, D. Theoretical evaluation of voltage inducement on internal membranes of biological cells exposed to electric fields. *Biophys. J.* **2006**, *90*, 480–491. [CrossRef]
47. Schoenbach, K.H.; Abou-Ghazala, A.; Vithoulkas, T.; Alden, R.W.; Turner, R.; Beebe, S. The effect of pulsed electrical fields on biological cells. In Digest of Technical Papers, Proceedings of the 11th IEEE International Pulsed Power Conference (Cat. No. 97CH36127), Baltimore, MD, USA, 29 June–2 July 1997; IEEE: Piscataway, NJ, USA, 1997, Volume 1, pp. 73–78.
48. Gowrishankar, T.R.; Esser, A.T.; Vasilkoski, Z.; Smith, K.C.; Weaver, J.C. Microdosimetry for conventional and supra-electroporation in cells with organelles. *Biochem. Biophys. Res. Commun.* **2006**, *341*, 1266–1276. [CrossRef]
49. Müller, K.; Sukhorukov, V.; Zimmermann, U. Reversible electropermeabilization of mammalian cells by high-intensity, ultra-short pulses of submicrosecond duration. *J. Membr. Biol.* **2001**, *184*, 161–170. [CrossRef] [PubMed]
50. Schoenbach, K.H.; Beebe, S.J.; Buescher, E.S. Intracellular effect of ultrashort electrical pulses. *Bioelectromagn. J. Bioelectromagn. Soc. Soc. Phys. Regul. Biol. Med. Eur. Bioelectromagn. Assoc.* **2001**, *22*, 440–448. [CrossRef] [PubMed]
51. White, J.A.; Blackmore, P.F.; Schoenbach, K.H.; Beebe, S.J. Stimulation of capacitative calcium entry in HL-60 cells by nanosecond pulsed electric fields. *J. Biol. Chem.* **2004**, *279*, 22964–22972. [CrossRef] [PubMed]

52. Vernier, P.T.; Sun, Y.; Chen, M.T.; Gundersen, M.A.; Craviso, G.L. Nanosecond electric pulse-induced calcium entry into chromaffin cells. *Bioelectrochemistry* **2008**, *73*, 1–4. [CrossRef]
53. Pakhomov, A.G.; Kolb, J.F.; White, J.A.; Joshi, R.P.; Xiao, S.; Schoenbach, K.H. Long-lasting plasma membrane permeabilization in mammalian cells by nanosecond pulsed electric field (nsPEF). *Bioelectromagn. J. Bioelectromagn. Soc. Soc. Phys. Regul. Biol. Med. Eur. Bioelectromagn. Assoc.* **2007**, *28*, 655–663. [CrossRef]
54. Cooper, R.A. Influence of increased membrane cholesterol on membrane fluidity and cell function in human red blood cells. *J. Supramol. Struct.* **1978**, *8*, 413–430. [CrossRef]
55. Minto, R.E.; Adhikari, P.R.; Lorigan, G.A. A 2H solid-state NMR spectroscopic investigation of biomimetic bicelles containing cholesterol and polyunsaturated phosphatidylcholine. *Chem. Phys. Lipids* **2004**, *132*, 55–64. [CrossRef]
56. Kusumi, A.; Tsuda, M.; Akino, T.; Ohnishi, S.; Terayama, Y. Protein-phospholipid-cholesterol interaction in the photolysis of invertebrate rhodopsin. *Biochemistry* **1983**, *22*, 1165–1170. [CrossRef]
57. McMullen, T.P.; McElhaney, R.N. Physical studies of cholesterol-phospholipid interactions. *Curr. Opin. Colloid Interface Sci.* **1996**, *1*, 83–90. [CrossRef]
58. Lu, J.X.; Caporini, M.A.; Lorigan, G.A. The effects of cholesterol on magnetically aligned phospholipid bilayers: A solid-state NMR and EPR spectroscopy study. *J. Magn. Reson.* **2004**, *168*, 18–30. [CrossRef]
59. Tiburu, E.K.; Dave, P.C.; Lorigan, G.A. Solid-state 2H NMR studies of the effects of cholesterol on the acyl chain dynamics of magnetically aligned phospholipid bilayers. *Magn. Reson. Chem.* **2004**, *42*, 132–138. [CrossRef] [PubMed]
60. Mason, R.P.; Tulenko, T.N.; Jacob, R.F. Direct evidence for cholesterol crystalline domains in biological membranes: Role in human pathobiology. *Biochim. Biophys. Acta (BBA)-Biomembr.* **2003**, *1610*, 198–207. [CrossRef]
61. Lund-Katz, S. Laboda, H.M.; McLean, L.R.; Phillips, M.C. Influence of molecular packing and phospholipid type on rates of cholesterol exchange. *Biochemistry* **1988**, *27*, 3416–3423. [CrossRef]
62. Smaby, J.M.; Brockman, H.L.; Brown, R.E. Cholesterol's interfacial interactions with sphingomyelins and-phosphatidylcholines: Hydrocarbon chain structure determines the magnitude of condensation. *Biochemistry* **1994**, *33*, 9135–9142. [CrossRef]
63. Anderson, T.G.; McConnell, H.M. Condensed complexes and the calorimetry of cholesterol-phospholipid bilayers. *Biophys. J.* **2001**, *81*, 2774–2785. [CrossRef]
64. Okonogi, T.; McConnell, H. Contrast inversion in the epifluorescence of cholesterol-phospholipid monolayers. *Biophys. J.* **2004**, *86*, 880–890. [CrossRef]
65. Evans, E.; Needham, D. Physical properties of surfactant bilayer membranes: Thermal transitions, elasticity, rigidity, cohesion and colloidal interactions. *J. Phys. Chem.* **1987**, *91*, 4219–4228. [CrossRef]
66. Needham, D.; McIntosh, T.; Evans, E. Thermomechanical and transition properties of dimyristoylphosphatidylcholine/cholesterol bilayers. *Biochemistry* **1988**, *27*, 4668–4673. [CrossRef]
67. Subczynski, W.K.; Wisniewska, A.; Yin, J.J.; Hyde, J.S.; Kusumi, A. Hydrophobic barriers of lipid bilayer membranes formed by reduction of water penetration by alkyl chain unsaturation and cholesterol. *Biochemistry* **1994**, *33*, 7670–7681. [CrossRef]
68. Bloom, M.; Mouritsen, O.G. The evolution of membranes. *Can. J. Chem.* **1988**, *66*, 706–712. [CrossRef]
69. Smondyrev, A.M.; Berkowitz, M.L. Structure of dipalmitoylphosphatidylcholine/cholesterol bilayer at low and high cholesterol concentrations: Molecular dynamics simulation. *Biophys. J.* **1999**, *77*, 2075–2089. [CrossRef]
70. Needham, D.; Nunn, R.S. Elastic deformation and failure of lipid bilayer membranes containing cholesterol. *Biophys. J.* **1990**, *58*, 997–1009. [CrossRef]
71. Portet, T.; Dimova, R. A new method for measuring edge tensions and stability of lipid bilayers: Effect of membrane composition. *Biophys. J.* **2010**, *99*, 3264–3273. [CrossRef] [PubMed]
72. Mattei, B.; Lira, R.B.; Perez, K.R.; Riske, K.A. Membrane permeabilization induced by Triton X-100: The role of membrane phase state and edge tension. *Chem. Phys. Lipids* **2017**, *202*, 28–37. [CrossRef] [PubMed]
73. Song, J.; Waugh, R.E. Bending rigidity of SOPC membranes containing cholesterol. *Biophys. J.* **1993**, *64*, 1967–1970. [CrossRef]
74. Evans, E.; Rawicz, W. Entropy-driven tension and bending elasticity in condensed-fluid membranes. *Phys. Rev. Lett.* **1990**, *64*, 2094. [CrossRef]
75. Petelska, A.D.; Naumowicz, M.; Figaszewski, Z.A. The interfacial tension of the lipid membrane formed from lipid-cholesterol and lipid-lipid systems. *Cell Biochem. Biophys.* **2006**, *44*, 205–211. [CrossRef]
76. Naumowicz, M.; Petelska, A.D.; Figaszewski, Z.A. Capacitance and resistance of the bilayer lipid membrane formed of phosphatidylcholine and cholesterol. *Cell. Mol. Biol. Lett.* **2003**, *8*, 5–18.
77. Shmygol, A.; Noble, K.; Wray, S. Depletion of membrane cholesterol eliminates the Ca^{2+}-activated component of outward potassium current and decreases membrane capacitance in rat uterine myocytes. *J. Physiol.* **2007**, *581*, 445–456. [CrossRef]
78. Levitan, I.; Christian, A.E.; Tulenko, T.N.; Rothblat, G.H. Membrane cholesterol content modulates activation of volume-regulated anion current in bovine endothelial cells. *J. Gen. Physiol.* **2000**, *115*, 405–416. [CrossRef]
79. Naumowicz, M.; Figaszewski, Z.A. Pore formation in lipid bilayer membranes made of phosphatidylcholine and cholesterol followed by means of constant current. *Cell Biochem. Biophys.* **2013**, *66*, 109–119. [CrossRef] [PubMed]
80. Goncharenko, M.; Katkov, I. Effect of cholesterol on the stability of human erythrocyte membranes to electric breakdown. *Biofizika* **1985**, *30*, 441–445. [PubMed]
81. Raffy, S.; Teissie, J. Control of lipid membrane stability by cholesterol content. *Biophys. J.* **1999**, *76*, 2072–2080. [CrossRef]

82. Needham, D.; Hochmuth, R. Electro-mechanical permeabilization of lipid vesicles. Role of membrane tension and compressibility. *Biophys. J.* **1989**, *55*, 1001–1009. [CrossRef]
83. Koronkiewicz, S.; Kalinowski, S. Influence of cholesterol on electroporation of bilayer lipid membranes: Chronopotentiometric studies. *Biochim. Biophys. Acta (BBA)-Biomembr.* **2004**, *1661*, 196–203. [CrossRef]
84. Casciola, M.; Bonhenry, D.; Liberti, M.; Apollonio, F.; Tarek, M. A molecular dynamic study of cholesterol rich lipid membranes: comparison of electroporation protocols. *Bioelectrochemistry* **2014**, *100*, 11–17. [CrossRef]
85. Koronkiewicz, S.; Kalinowski, S.; Bryl, K. Programmable chronopotentiometry as a tool for the study of electroporation and resealing of pores in bilayer lipid membranes. *Biochim. Biophys. Acta (BBA)-Biomembr.* **2002**, *1561*, 222–229. [CrossRef]
86. Kalinowski, S.; Ibron, G.; Bryl, K.; Figaszewski, Z. Chronopotentiometric studies of electroporation of bilayer lipid membranes. *Biochim. Biophys. Acta (BBA)-Biomembr.* **1998**, *1369*, 204–212. [CrossRef]
87. Coster, H.G. Dielectric and Electrical Properties of Lipid Bilayers in Relation to their Structure. In *Membrane Science and Technology*; Elsevier: Amsterdam, The Netherlands, 2003; Volume 7, pp. 75–108.
88. McIntosh, T.J. The effect of cholesterol on the structure of phosphatidylcholine bilayers. *Biochim. Biophys. Acta (BBA)-Biomembr.* **1978**, *513*, 43–58. [CrossRef]
89. Cantu, J.C.; Tarango, M.; Beier, H.T.; Ibey, B.L. The biological response of cells to nanosecond pulsed electric fields is dependent on plasma membrane cholesterol. *Biochim. Biophys. Acta (BBA)-Biomembr.* **2016**, *1858*, 2636–2646. [CrossRef]
90. Ullery, J.C.; Beier, H.T.; Ibey, B.L. Sensitivity of Cells to Nanosecond Pulsed Electric Fields is Dependent on Membrane Lipid Microdomains. In Proceedings of the 1st World Congress on Electroporation and Pulsed Electric Fields in Biology, Medicine and Food & Environmental Technologies, Portorož, Slovenia, 6–10 September 2015; pp. 239–242.
91. Hu, Q.; Joshi, R.; Schoenbach, K. Simulations of nanopore formation and phosphatidylserine externalization in lipid membranes subjected to a high-intensity, ultrashort electric pulse. *Phys. Rev. E* **2005**, *72*, 031902. [CrossRef] [PubMed]
92. Zimmermann, U.; Neil, G.A. *Electromanipulation of Cells*; CRC Press: Boca Raton, FL, USA, 1996.
93. Kolb, J.F.; Kono, S.; Schoenbach, K.H. Nanosecond pulsed electric field generators for the study of subcellular effects. *Bioelectromagnetics* **2006**, *27*, 172–187. [CrossRef] [PubMed]
94. Schoenbach, K.H.; Joshi, R.P.; Beebe, S.J.; Baum, C.E. A scaling law for membrane permeabilization with nanopulses. *IEEE Trans. Dielectr. Electr. Insul.* **2009**, *16*, 1224–1235. [CrossRef]
95. Vernier, P.T.; Sun, Y.; Marcu, L.; Salemi, S.; Craft, C.M.; Gundersen, M.A. Calcium bursts induced by nanosecond electric pulses. *Biochem. Biophys. Res. Commun.* **2003**, *310*, 286–295. [CrossRef] [PubMed]
96. Koch, C.; Rapp, M.; Segev, I. A brief history of time (constants). *Cereb. Cortex* **1996**, *6*, 93–101. [CrossRef] [PubMed]
97. Molitor, S.C.; Manis, P.B. Voltage-gated Ca^{2+} conductances in acutely isolated guinea pig dorsal cochlear nucleus neurons. *J. Neurophysiol.* **1999**, *81*, 985–998. [CrossRef] [PubMed]
98. Hille, B. *Ion Channels of Excitable Membranes*; Sinauer: Sunderland, MA, USA, 2001; Volume 507.
99. Zagotta, W.N.; Hoshi, T.; Aldrich, R.W. Shaker potassium channel gating. III: Evaluation of kinetic models for activation. *J. Gen. Physiol.* **1994**, *103*, 321–362. [CrossRef]
100. Baker, O.; Larsson, H.; Mannuzzu, L.; Isacoff, E. Three transmembrane conformations and sequence-dependent displacement of the S4 domain in shaker K^+ channel gating. *Neuron* **1998**, *20*, 1283–1294. [CrossRef]
101. Sigg, D.; Bezanilla, F.; Stefani, E. Fast gating in the Shaker K^+ channel and the energy landscape of activation. *Proc. Natl. Acad. Sci. USA* **2003**, *100*, 7611–7615. [CrossRef]
102. Blaustein, R.O.; Miller, C. Ion channels: Shake, rattle or roll? *Nature* **2004**, *427*, 499. [CrossRef]
103. Horn, R. Conversation between voltage sensors and gates of ion channels. *Biochemistry* **2000**, *39*, 15653–15658. [CrossRef] [PubMed]
104. Catterall, W.A. Voltage-dependent gating of sodium channels: Correlating structure and function. *Trends Neurosci.* **1986**, *9*, 7–10. [CrossRef]
105. GuY, H.R.; Seetharamulu, P. Molecular model of the action potential sodium channel. *Proc. Natl. Acad. Sci. USA* **1986**, *83*, 508–512. [CrossRef] [PubMed]
106. Bezanilla, F. The voltage sensor in voltage-dependent ion channels. *Physiol. Rev.* **2000**, *80*, 555–592. [CrossRef] [PubMed]
107. Jiang, Y.; Ruta, V.; Chen, J.; Lee, A.; MacKinnon, R. The principle of gating charge movement in a voltage-dependent K^+ channel. *Nature* **2003**, *423*, 42–48. [CrossRef]
108. Jiang, Y.; Lee, A.; Chen, J.; Ruta, V.; Cadene, M.; Chait, B.T.; MacKinnon, R. X-ray structure of a voltage-dependent K^+ channel. *Nature* **2003**, *423*, 33. [CrossRef]
109. Chanda, B.; Asamoah, O.K.; Blunck, R.; Roux, B.; Bezanilla, F. Gating charge displacement in voltage-gated ion channels involves limited transmembrane movement. *Nature* **2005**, *436*, 852–856. [CrossRef]
110. Auld, V.; Marshall, J.; Goldin, A.; Dowsett, A.; Catterall, W.; Davidson, N.; Dunn, R. Cloning and characterization of the gene for alpha-subunit of the mammalian voltage-gated sodium-channel. *J. Gen. Physiol.* **1985**, *86*, A10–A11.
111. Noda, M. Shimizu, S.; Tanabe, T.; Takai, T.; Kayano, T.; Ikeda, T.; Takahashi, H.; Nakayama, H.; Kanaoka, Y.; Minamino, N. Primary structure of Electrophorus electricus sodium channel deduced from cDNA sequence. *Nature* **1984**, *312*, 121–127. [CrossRef]
112. Wu, D.; Delaloye, K.; Zaydman, M.A.; Nekouzadeh, A.; Rudy, Y.; Cui, J. State-dependent electrostatic interactions of S4 arginines with E1 in S2 during Kv7. 1 activation. *J. Gen. Physiol.* **2010**, *135*, 595–606. [CrossRef]

113. DeCaen, P.G.; Yarov-Yarovoy, V.; Sharp, E.M.; Scheuer, T.; Catterall, W.A. Sequential formation of ion pairs during activation of a sodium channel voltage sensor. *Proc. Natl. Acad. Sci. USA* **2009**, *106*, 22498–22503. [CrossRef] [PubMed]
114. Tao, X.; Lee, A.; Limapichat, W.; Dougherty, D.A.; MacKinnon, R. A gating charge transfer center in voltage sensors. *Science* **2010**, *328*, 67–73. [CrossRef] [PubMed]
115. Perozo, E.; Cortes, D.M.; Cuello, L.G. Three-dimensional architecture and gating mechanism of a K^+ channel studied by EPR spectroscopy. *Nat. Struct. Biol.* **1998**, *5*, 459–469. [CrossRef] [PubMed]
116. Perozo, E.; Marien, D.; Cuello, L.G. Structural rearrangements underlying K^+-channel activation gating. *Science* **1999**, *285*, 73–78. [CrossRef]
117. Seoh, S.A.; Sigg, D.; Papazian, D.M.; Bezanilla, F. Voltage-sensing residues in the S2 and S4 segments of the Shaker K^+ channel. *Neuron* **1996**, *16*, 1159–1167. [CrossRef]
118. Aggarwal, S.K.; MacKinnon, R. Contribution of the S4 segment to gating charge in the Shaker K^+ channel. *Neuron* **1996**, *16*, 1169–1177. [CrossRef]
119. Schoppa, N.E.; McCormack, K.; Tanouye, M.A.; Sigworth, F.J. The size of gating charge in wild-type and mutant Shaker potassium channels. *Science* **1992**, *255*, 1712–1715. [CrossRef]
120. Starace, D.M.; Bezanilla, F. A proton pore in a potassium channel voltage sensor reveals a focused electric field. *Nature* **2004**, *427*, 548–553. [CrossRef]
121. Asamoah, O.K.; Wuskell, J.P.; Loew, L.M.; Bezanilla, F. A fluorometric approach to local electric field measurements in a voltage-gated ion channel. *Neuron* **2003**, *37*, 85–98. [CrossRef]
122. Jensen, M.Ø.; Jogini, V.; Borhani, D.W.; Leffler, A.E.; Dror, R.O.; Shaw, D.E. Mechanism of voltage gating in potassium channels. *Science* **2012**, *336*, 229–233. [CrossRef]
123. Payandeh, J.; Scheuer, T.; Zheng, N.; Catterall, W.A. The crystal structure of a voltage-gated sodium channel. *Nature* **2011**, *475*, 353. [CrossRef] [PubMed]
124. Zhang, X.; Ren, W.; DeCaen, P.; Yan, C.; Tao, X.; Tang, L.; Wang, J.; Hasegawa, K.; Kumasaka, T.; He, J.; et al. Crystal structure of an orthologue of the NaChBac voltage gated sodium channel. *Nature* **2012**, *486*, 130–134. [CrossRef] [PubMed]
125. Yarov-Yarovoy, V.; Baker, D.; Catterall, W.A. Voltage sensor conformations in the open and closed states in ROSETTA structural models of K^+ channels. *Proc. Natl. Acad. Sci. USA* **2006**, *103*, 7292–7297. [CrossRef] [PubMed]
126. Yarov-Yarovoy, V.; DeCaen, P.G.; Westenbroek, R.E.; Pan, C.Y.; Scheuer, T.; Baker, D.; Catterall, W.A. Structural basis for gating charge movement in the voltage sensor of a sodium channel. *Proc. Natl. Acad. Sci. USA* **2012**, *109*, E93–E102. [CrossRef]
127. Pathak, M.M.; Yarov-Yarovoy, V.; Agarwal, G.; Roux, B.; Barth, P.; Kohout, S.; Tombola, F.; Isacoff, E.Y. Closing in on the resting state of the Shaker K^+ channel. *Neuron* **2007**, *56*, 124–140. [CrossRef]
128. Delemotte, L.; Treptow, W.; Klein, M.L.; Tarek, M. Effect of sensor domain mutations on the properties of voltage-gated ion channels: Molecular dynamics studies of the potassium channel Kv1. 2. *Biophys. J.* **2010**, *99*, L72–L74. [CrossRef]
129. Khalili-Araghi, F.; Jogini, V.; Yarov-Yarovoy, V.; Tajkhorshid, E.; Roux, B.; Schulten, K. Calculation of the gating charge for the Kv1. 2 voltage-activated potassium channel. *Biophys. J.* **2010**, *98*, 2189–2198. [CrossRef]
130. Henrion, U.; Renhorn, J.; Börjesson, S.I.; Nelson, E.M.; Schwaiger, C.S.; Bjelkmar, P.; Wallner, B.; Lindahl, E.; Elinder, F. Tracking a complete voltage-sensor cycle with metal-ion bridges. *Proc. Natl. Acad. Sci. USA* **2012**, *109*, 8552–8557. [CrossRef]
131. Baukrowitz, T.; Yellen, G. Two functionally distinct subsites for the binding of internal blockers to the pore of voltage-activated K^+ channels. *Proc. Natl. Acad. Sci. USA* **1996**, *93*, 13357–13361. [CrossRef]
132. Baukrowitz, T.; Yellen, G. Use-dependent blockers and exit rate of the last ion from the multi-ion pore of a K^+ channel. *Science* **1996**, *271*, 653–656. [CrossRef]
133. Ray, E.C.; Deutsch, C. A trapped intracellular cation modulates K^+ channel recovery from slow inactivation. *J. Gen. Physiol.* **2006**, *128*, 203–217. [CrossRef]
134. Payandeh, J.; El-Din, T.M.G.; Scheuer, T.; Zheng, N.; Catterall, W.A. Crystal structure of a voltage-gated sodium channel in two potentially inactivated states. *Nature* **2012**, *486*, 135–139. [CrossRef]
135. Sachs, J.N.; Crozier, P.S.; Woolf, T.B. Atomistic simulations of biologically realistic transmembrane potential gradients. *J. Chem. Phys.* **2004**, *121*, 10847–10851. [CrossRef]
136. Delemotte, L.; Dehez, F.; Treptow, W.; Tarek, M. Modeling membranes under a transmembrane potential. *J. Phys. Chem. B* **2008**, *112*, 5547–5550. [CrossRef]
137. Roux, B. The membrane potential and its representation by a constant electric field in computer simulations. *Biophys. J.* **2008**, *95*, 4205–4216. [CrossRef]
138. Dzubiella, J.; Allen, R.; Hansen, J.P. Electric field-controlled water permeation coupled to ion transport through a nanopore. *J. Chem. Phys.* **2004**, *120*, 5001–5004. [CrossRef]
139. Beebe, S.J.; Fox, P.; Rec, L.; Somers, K.; Stark, R.H.; Schoenbach, K.H. Nanosecond pulsed electric field (nsPEF) effects on cells and tissues: Apoptosis induction and tumor growth inhibition. *IEEE Trans. Plasma Sci.* **2002**, *30*, 286–292. [CrossRef]
140. Armstrong, C.; Matteson, D. Two distinct populations of calcium channels in a clonal line of pituitary cells. *Science* **1985**, *227*, 65–67. [CrossRef]
141. Bean, B.P. Two kinds of calcium channels in canine atrial cells. Differences in kinetics, selectivity, and pharmacology. *J. Gen. Physiol.* **1985**, *86*, 1–30. [CrossRef]

142. Curtis, B.M.; Catterall, W.A. Purification of the calcium antagonist receptor of the voltage-sensitive calcium channel from skeletal muscle transverse tubules. *Biochemistry* **1984**, *23*, 2113–2118. [CrossRef]
143. Catterall, W.A.; Perez-Reyes, E.; Snutch, T.P.; Striessnig, J. International Union of Pharmacology. XLVIII. Nomenclature and structure-function relationships of voltage-gated calcium channels. *Pharmacol. Rev.* **2005**, *57*, 411–425. [CrossRef]
144. Bech-Hansen, N.T.; Naylor, M.J.; Maybaum, T.A.; Pearce, W.G.; Koop, B.; Fishman, G.A.; Mets, M.; Musarella, M.A.; Boycott, K.M. Loss-of-function mutations in a calcium-channel α 1-subunit gene in Xp11. 23 cause incomplete X-linked congenital stationary night blindness. *Nat. Genet.* **1998**, *19*, 264. [CrossRef]
145. Mikami, A.; Imoto, K.; Tanabe, T.; Niidome, T.; Mori, Y.; Takeshima, H.; Narumiya, S.; Numa, S. Primary structure and functional expression of the cardiac dihydropyridine-sensitive calcium channel. *Nature* **1989**, *340*, 230. [CrossRef]
146. Tanabe, T.; Takeshima, H.; Mikami, A.; Flockerzi, V.; Takahashi, H.; Kangawa, K.; Kojima, M.; Matsuo, H.; Hirose, T.; Numa, S. Primary structure of the receptor for calcium channel blockers from skeletal muscle. *Nature* **1987**, *328*, 313. [CrossRef]
147. Williams, M.E.; Feldman, D.H.; McCue, A.F.; Brenner, R.; Velicelebi, G.; Ellis, S.B.; Harpold, M.M. Structure and functional expression of α1, α2, and β subunits of a novel human neuronal calcium channel subtype. *Neuron* **1992**, *8*, 71–84. [CrossRef]
148. Randall, A.; Tsien, R.W. Pharmacological dissection of multiple types of Ca^{2+} channel currents in rat cerebellar granule neurons. *J. Neurosci.* **1995**, *15*, 2995–3012. [CrossRef]
149. Bourinet, E.; Soong, T.W.; Sutton, K.; Slaymaker, S.; Mathews, E.; Monteil, A.; Zamponi, G.W.; Nargeot, J.; Snutch, T.P. Splicing of α 1A subunit gene generates phenotypic variants of P-and Q-type calcium channels. *Nat. Neurosci.* **1999**, *2*, 407. [CrossRef]
150. Richards, K.S.; Swensen, A.M.; Lipscombe, D.; Bommert, K. Novel CaV2. 1 clone replicates many properties of Purkinje cell CaV2. 1 current. *Eur. J. Neurosci.* **2007**, *26*, 2950–2961. [CrossRef]
151. Adams, M.E.; Myers, R.A.; Imperial, J.S.; Olivera, B.M. Toxityping rat brain calcium channels with. omega.-toxins from spider and cone snail venoms. *Biochemistry* **1993**, *32*, 12566–12570. [CrossRef]
152. Dubel, S.J.; Starr, T.; Hell, J.; Ahlijanian, M.K.; Enyeart, J.J.; Catterall, W.A.; Snutch, T.P. Molecular cloning of the alpha-1 subunit of an omega-conotoxin-sensitive calcium channel. *Proc. Natl. Acad. Sci. USA* **1992**, *89*, 5058–5062. [CrossRef]
153. Soong, T.W.; Stea, A.; Hodson, C.D.; Dubel, S.J.; Vincent, S.R.; Snutch, T.P. Structure and functional expression of a member of the low voltage-activated calcium channel family. *Science* **1993**, *260*, 1133–1136. [CrossRef] [PubMed]
154. Bourinet, E.; Stotz, S.C.; Spaetgens, R.L.; Dayanithi, G.; Lemos, J.; Nargeot, J.; Zamponi, G.W. Interaction of SNX482 with domains III and IV inhibits activation gating of α1E (CaV2. 3) calcium channels. *Biophys. J.* **2001**, *81*, 79–88. [CrossRef]
155. Newcomb, R.; Szoke, B.; Palma, A.; Wang, G.; Chen, X.; Hopkins, W.; Cong, R.; Miller, J.; Urge, L.; Tarczy-Hornoch, K.; et al. Selective peptide antagonist of the class E calcium channel from the venom of the tarantula Hysterocrates gigas. *Biochemistry* **1998**, *37*, 15353–15362. [CrossRef]
156. Cribbs, L.L.; Lee, J.H.; Yang, J.; Satin, J.; Zhang, Y.; Daud, A.; Barclay, J.; Williamson, M.P.; Fox, M.; Rees, M.; et al. Cloning and characterization of α1H from human heart, a member of the T-type Ca^{2+} channel gene family. *Circ. Res.* **1998**, *83*, 103–109. [CrossRef] [PubMed]
157. Lee, J.H.; Daud, A.N.; Cribbs, L.L.; Lacerda, A.E.; Pereverzev, A.; Klöckner, U.; Schneider, T.; Perez-Reyes, E. Cloning and expression of a novel member of the low voltage-activated T-type calcium channel family. *J. Neurosci.* **1999**, *19*, 1912–1921. [CrossRef] [PubMed]
158. Perez-Reyes, E.; Cribbs, L.L.; Daud, A.; Lacerda, A.E.; Barclay, J.; Williamson, M.P.; Fox, M.; Rees, M.; Lee, J.H. Molecular characterization of a neuronal low-voltage-activated T-type calcium channel. *Nature* **1998**, *391*, 896. [CrossRef]
159. Perez-Reyes, E. Molecular physiology of low-voltage-activated t-type calcium channels. *Physiol. Rev.* **2003**, *83*, 117–161. [CrossRef]
160. Catterall, W.A. Ion channel voltage sensors: Structure, function, and pathophysiology. *Neuron* **2010**, *67*, 915–928. [CrossRef]
161. Ellinor, P.T.; Yang, J.; Sather, W.A.; Zhang, J.F.; Tsien, R.W. Ca^{2+} channel selectivity at a single locus for high-affinity Ca^{2+} interactions. *Neuron* **1995**, *15*, 1121–1132. [CrossRef]
162. Tang, L.; El-Din, T.M.G.; Payandeh, J.; Martinez, G.Q.; Heard, T.M.; Scheuer, T.; Zheng, N.; Catterall, W.A. Structural basis for Ca^{2+} selectivity of a voltage-gated calcium channel. *Nature* **2014**, *505*, 56. [CrossRef]
163. Yang, J.; Elllnor, P.T.; Sather, W.A.; Zhang, J.F.; Tsien, R.W. Molecular determinants of Ca^{2+} selectivity and ion permeation in L-type Ca^{2+} channels. *Nature* **1993**, *366*, 158. [CrossRef] [PubMed]
164. Bourinet, E.; Zamponi, G.W.; Stea, A.; Soong, T.W.; Lewis, B.A.; Jones, L.P.; Yue, D.T.; Snutch, T.P. The α1E calcium channel exhibits permeation properties similar to low-voltage-activated calcium channels. *J. Neurosci.* **1996**, *16*, 4983–4993. [CrossRef] [PubMed]
165. Lansman, J.B.; Hess, P.; Tsien, R.W. Blockade of current through single calcium channels by Cd^{2+}, Mg^{2+}, and Ca^{2+}. Voltage and concentration dependence of calcium entry into the pore. *J. Gen. Physiol.* **1986**, *88*, 321–347. [CrossRef] [PubMed]
166. Chen, Y.h.; Li, M.h.; Zhang, Y.; He, L.l.; Yamada, Y.; Fitzmaurice, A.; Shen, Y.; Zhang, H.; Tong, L.; Yang, J. Structural basis of the α $1-\beta$ subunit interaction of voltage-gated Ca^{2+} channels. *Nature* **2004**, *429*, 675. [CrossRef] [PubMed]
167. Van Petegem, F.; Clark, K.A.; Chatelain, F.C.; Minor, D.L., Jr. Structure of a complex between a voltage-gated calcium channel β-subunit and an α-subunit domain. *Nature* **2004**, *429*, 671. [CrossRef] [PubMed]
168. Fallon, J.L.; Halling, D.B.; Hamilton, S.L.; Quiocho, F.A. Structure of calmodulin bound to the hydrophobic IQ domain of the cardiac Cav1. 2 calcium channel. *Structure* **2005**, *13*, 1881–1886. [CrossRef]

169. Fallon, J.L.; Baker, M.R.; Xiong, L.; Loy, R.E.; Yang, G.; Dirksen, R.T.; Hamilton, S.L.; Quiocho, F.A. Crystal structure of dimeric cardiac L-type calcium channel regulatory domains bridged by Ca^{2+}· calmodulins. *Proc. Natl. Acad. Sci. USA* **2009**, *106*, 5135–5140. [CrossRef]
170. Kim, E.Y.; Rumpf, C.H.; Fujiwara, Y.; Cooley, E.S.; Van Petegem, F.; Minor, D.L., Jr. Structures of CaV2 Ca^{2+}/CaM-IQ domain complexes reveal binding modes that underlie calcium-dependent inactivation and facilitation. *Structure* **2008**, *16*, 1455–1467. [CrossRef]
171. Kim, E.Y.; Rumpf, C.H.; Van Petegem, F.; Arant, R.J.; Findeisen, F.; Cooley, E.S.; Isacoff, E.Y.; Minor, D.L. Multiple C-terminal tail Ca^{2+}/CaMs regulate CaV1. 2 function but do not mediate channel dimerization. *EMBO J.* **2010**, *29*, 3924–3938. [CrossRef]
172. Liu, Z.; Vogel, H. Structural basis for the regulation of L-type voltage-gated calcium channels: Interactions between the N-terminal cytoplasmic domain and Ca^{2+}-calmodulin. *Front. Mol. Neurosci.* **2012**, *5*, 38. [CrossRef]
173. Mori, M.; Vander Kooi, C.; Leahy, D.; Yue, D. Structure of the CaV2 IQ domain in complex with Ca^{2+}/calmodulin. In Proceedings of the Annual Meeting of the Physiological Society of Japan, Virtual Event, 3 April 2008; p. 072.
174. Van Petegem, F.; Chatelain, F.C.; Minor Jr, D.L. Insights into voltage-gated calcium channel regulation from the structure of the Ca V 1.2 IQ domain–Ca^{2+}/calmodulin complex. *Nat. Struct. Mol. Biol.* **2005**, *12*, 1108. [CrossRef] [PubMed]
175. Serysheva, I.; Ludtke, S.; Baker, M.; Chiu, W.; Hamilton, S. Structure of the voltage-gated L-type Ca^{2+} channel by electron cryomicroscopy. *Proc. Natl. Acad. Sci. USA* **2002**, *99*, 10370–10375. [CrossRef] [PubMed]
176. Walsh, C.P.; Davies, A.; Butcher, A.J.; Dolphin, A.C.; Kitmitto, A. Three-dimensional Structure of CaV3. 1 comparison with the cardiac l-type voltage-gated calcium channel monomer architecture. *J. Biol. Chem.* **2009**, *284*, 22310–22321. [CrossRef] [PubMed]
177. Walsh, C.P.; Davies, A.; Nieto-Rostro, M.; Dolphin, A.C.; Kitmitto, A. Labelling of the 3D structure of the cardiac L-type voltage-gated calcium channel. *Channels* **2009**, *3*, 387–392. [CrossRef] [PubMed]
178. Wolf, M.; Eberhart, A.; Glossmann, H.; Striessnig, J.; Grigorieff, N. Visualization of the domain structure of an L-type Ca^{2+} channel using electron cryo-microscopy. *J. Mol. Biol.* **2003**, *332*, 171–182. [CrossRef]
179. Long, S.B.; Campbell, E.B.; MacKinnon, R. Crystal structure of a mammalian voltage-dependent Shaker family K^+ channel. *Science* **2005**, *309*, 897–903. [CrossRef]
180. Huber, I.; Wappl, E.; Herzog, A.; Mitterdorfer, J.; Glossmann, H.; Langer, T.; Striessnig, J. Conserved Ca^{2+}-antagonist-binding properties and putative folding structure of a recombinant high-affinity dihydropyridine-binding domain. *Biochem. J.* **2000**, *347*, 829–836. [CrossRef]
181. Lipkind, G.M.; Fozzard, H.A. Molecular modeling of interactions of dihydropyridines and phenylalkylamines with the inner pore of the L-type Ca^{2+} channel. *Mol. Pharmacol.* **2003**, *63*, 499–511. [CrossRef]
182. Zamponi, G.W.; Stotz, S.C.; Staples, R.J.; Andro, T.M.; Nelson, J.K.; Hulubei, V.; Blumenfeld, A.; Natale, N.R. Unique structure-activity relationship for 4-isoxazolyl-1, 4-dihydropyridines. *J. Med. Chem.* **2003**, *46*, 87–96. [CrossRef]
183. Delemotte, L.; Tarek, M.; Klein, M.L.; Amaral, C.; Treptow, W. Intermediate states of the Kv1. 2 voltage sensor from atomistic molecular dynamics simulations. *Proc. Natl. Acad. Sci. USA* **2011**, *108*, 6109–6114. [CrossRef]
184. Simms, B.A.; Zamponi, G.W. Neuronal voltage-gated calcium channels: Structure, function, and dysfunction. *Elsevier* **2014**, *82*, 24–45. [CrossRef] [PubMed]
185. Rogers, W.R.; Merritt, J.H.; Comeaux, J.A.; Kuhnel, C.T.; Moreland, D.F.; Teltschik, D.G.; Lucas, J.H.; Murphy, M.R. Strength-duration curve for an electrically excitable tissue extended down to near 1 nanosecond. *IEEE Trans. Plasma Sci.* **2004**, *32*, 1587–1599. [CrossRef]
186. Craviso, G.L.; Choe, S.; Chatterjee, P.; Chatterjee, I.; Vernier, P.T. Nanosecond electric pulses: A novel stimulus for triggering Ca^{2+} influx into chromaffin cells via voltage-gated Ca^{2+} channels. *Cell. Mol. Neurobiol.* **2010**, *30*, 1259–1265. [CrossRef]
187. Burke, R.C.; Bardet, S.M.; Carr, L.; Romanenko, S.; Arnaud-Cormos, D.; Leveque, P.; O'Connor, R.P. Nanosecond pulsed electric fields depolarize transmembrane potential via voltage-gated K^+, Ca^{2+} and TRPM8 channels in U87 glioblastoma cells. *Biochim. Biophys. Acta (BBA)-Biomembr.* **2017**, *1859*, 2040–2050. [CrossRef] [PubMed]
188. Pakhomov, A.G.; Semenov, I.; Casciola, M.; Xiao, S. Neuronal excitation and permeabilization by 200-ns pulsed electric field: An optical membrane potential study with FluoVolt dye. *Biochim. Biophys. Acta (BBA)-Biomembr.* **2017**, *1859*, 1273–1281. [CrossRef]
189. Bagalkot, T.R.; Leblanc, N.; Craviso, G.L. Stimulation or Cancellation of Ca^{2+} Influx by Bipolar Nanosecond Pulsed Electric Fields in Adrenal Chromaffin Cells Can Be Achieved by Tuning Pulse Waveform. *Sci. Rep.* **2019**, *9*, 11545. [CrossRef]
190. Bagalkot, T.R.; Terhune, R.C.; Leblanc, N.; Craviso, G.L. Different membrane pathways mediate Ca^{2+} influx in adrenal chromaffin cells exposed to 150–400 ns electric pulses. *BioMed Res. Int.* **2018**, *2018*, 9046891 . [CrossRef]
191. Hristov, K.; Mangalanathan, U.; Casciola, M.; Pakhomova, O.N.; Pakhomov, A.G. Expression of voltage-gated calcium channels augments cell susceptibility to membrane disruption by nanosecond pulsed electric field. *Biochim. Biophys. Acta (BBA)-Biomembr.* **2018**, *1860*, 2175–2183. [CrossRef]
192. Esser, A.T.; Smith, K.C.; Gowrishankar, T.; Vasilkoski, Z.; Weaver, J.C. Mechanisms for the intracellular manipulation of organelles by conventional electroporation. *Biophys. J.* **2010**, *98*, 2506–2514. [CrossRef]
193. Kotnik, T.; Rems, L.; Tarek, M.; Miklavčič, D. Membrane electroporation and electropermeabilization: Mechanisms and models. *Annu. Rev. Biophys.* **2019**, *48*, 63–91. [CrossRef]
194. Teissie, J.; Tsong, T.Y. Evidence of voltage-induced channel opening in Na/K ATPase of human erythrocyte membrane. *J. Membr. Biol.* **1980**, *55*, 133–140. [CrossRef] [PubMed]

195. Tsong, T.Y. Electroporation of cell membranes. In *Electroporation and Electrofusion in Cell Biology*; Spring: Berlin/Heidelberg, Germany, 1989; pp. 149–163.
196. Marracino, P.; Bernardi, M.; Liberti, M.; Del Signore, F.; Trapani, E.; Garate, J.A.; Burnham, C.J.; Apollonio, F.; English, N.J. Transprotein-electropore characterization: A molecular dynamics investigation on human AQP4. *ACS Omega* **2018**, *3*, 15361–15369. [CrossRef] [PubMed]
197. Rems, L.; Kasimova, M.A.; Testa, I.; Delemotte, L. Pulsed electric fields can create pores in the voltage sensors of voltage-gated ion channels. *Biophys. J.* **2020**, *119*, 190–205. [CrossRef] [PubMed]
198. Weaver, J.C. Electroporation: A general phenomenon for manipulating cells and tissues. *J. Cell. Biochem.* **1993**, *51*, 426–435. [CrossRef] [PubMed]
199. Weaver, J.C.; Vernier, P.T. Pore lifetimes in cell electroporation: Complex dark pores? *arXiv* **2017**, arXiv:1708.07478.
200. Weaver, J.C.; Barnett, A. Progress toward a theoretical model for electroporation mechanism: Membrane electrical behavior and molecular transport. In *Guide to Electroporation and Electrofusion*; Spring: Berlin/Heidelberg, Germany, 1992; pp. 91–117.
201. Nesin, V.; Bowman, A.M.; Xiao, S.; Pakhomov, A.G. Cell permeabilization and inhibition of voltage-gated Ca^{2+} and Na^{+} channel currents by nanosecond pulsed electric field. *Bioelectromagnetics* **2012**, *33*, 394–404. [CrossRef]
202. Nesin, V.; Pakhomov, A.G. Inhibition of voltage-gated Na^{+} current by nanosecond pulsed electric field (nsPEF) is not mediated by Na^{+} influx or Ca^{2+} signaling. *Bioelectromagnetics* **2012**, *33*, 443–451. [CrossRef]
203. Yang, L.; Craviso, G.L.; Vernier, P.T.; Chatterjee, I.; Leblanc, N. Nanosecond electric pulses differentially affect inward and outward currents in patch clamped adrenal chromaffin cells. *PLoS ONE* **2017**, *12*, e0181002. [CrossRef]
204. Chen, W.; Han, Y.; Chen, Y.; Astumian, D. Electric field-induced functional reductions in the K^{+} channels mainly resulted from supramembrane potential-mediated electroconformational changes. *Biophys. J.* **1998**, *75*, 196–206. [CrossRef]
205. Levine, Z.A.; Vernier, P.T. Life cycle of an electropore: Field-dependent and field-independent steps in pore creation and annihilation. *J. Membr. Biol.* **2010**, *236*, 27–36. [CrossRef]
206. Bennett, W.D.; Sapay, N.; Tieleman, D.P. Atomistic simulations of pore formation and closure in lipid bilayers. *Biophys. J.* **2014**, *106*, 210–219. [CrossRef] [PubMed]
207. Ruiz-Fernández, A.R.; Campos, L.; Villanelo, F.; Gutiérrez-Maldonado, S.E.; Perez-Acle, T. Exploring the Conformational Changes Induced by Nanosecond Pulsed Electric Fields on the Voltage Sensing Domain of a Ca^{2+} Channel. *Membranes* **2021**, *11*, 473. [CrossRef] [PubMed]
208. Di Mattia, V.; Marracino, P.; Apollonio, F.; Liberti, M.; Amadei, A.; d'Inzeo, G. Molecular Dynamics Simulations of a Nanosecond E-Field Pulse Acting on Single DNA Strand. Available online: https://www.researchgate.net/profile/Andrea-Amadei-3/publication/228895176_Molecular_Dynamics_Simulations_of_a_Nanosecond_E-Field_Pulse_acting_on_Single_DNA_Strand/links/0912f509a6eb6b3492000000/Molecular-Dynamics-Simulations-of-a-Nanosecond-E-Field-Pulse-acting-on-Single-DNA-Strand.pdf (accessed on 27 April 2022).
209. Li, H.; Liu, S.; Yang, X.; Du, Y.; Luo, J.; Tan, J.; Sun, Y. Cellular Processes Involved in Jurkat Cells Exposed to Nanosecond Pulsed Electric Field. *Int. J. Mol. Sci.* **2019**, *20*, 5847. [CrossRef]
210. Wang, S.; Chen, J.; Chen, M.T.; Vernier, P.T.; Gundersen, M.A.; Valderrábano, M. Cardiac myocyte excitation by ultrashort high-field pulses. *Biophys. J.* **2009**, *96*, 1640–1648. [CrossRef]
211. Azarov, J.E.; Semenov, I.; Casciola, M.; Pakhomov, A.G. Excitation of murine cardiac myocytes by nanosecond pulsed electric field. *J. Cardiovasc. Electrophysiol.* **2019**, *30*, 392–401. [CrossRef] [PubMed]
212. Pakhomov, A.G.; Xiao, S.; Novickij, V.; Casciola, M.; Semenov, I.; Mangalanathan, U.; Kim, V.; Zemlin, C.; Sozer, E.; Muratori, C.; et al. Excitation and electroporation by MHz bursts of nanosecond stimuli. *Biochem. Biophys. Res. Commun.* **2019**, *518*, 759–764. [CrossRef]
213. Semenov, I.; Grigoryev, S.; Neuber, J.U.; Zemlin, C.W.; Pakhomova, O.N.; Casciola, M.; Pakhomov, A.G. Excitation and injury of adult ventricular cardiomyocytes by nano-to millisecond electric shocks. *Sci. Rep.* **2018**, *8*, 8233. [CrossRef]
214. Romanenko, S.; Arnaud-Cormos, D.; Leveque, P.; O'Connor, R.P. Ultrashort pulsed electric fields induce action potentials in neurons when applied at axon bundles. In Proceedings of the 2016 9th International Kharkiv Symposium on Physics and Engineering of Microwaves, Millimeter and Submillimeter Waves (MSMW), Kharkiv, Ukraine, 20–24 June 2016; pp. 1–5.
215. Casciola, M.; Xiao, S.; Pakhomov, A.G. Damage-free peripheral nerve stimulation by 12-ns pulsed electric field. *Sci. Rep.* **2017**, *7*, 10453. [CrossRef]
216. Lamberti, P.; Tucci, V.; Zeni, O.; Romeo, S. Analysis of ionic channel currents under nsPEFs-stimulation by a circuital model of an excitable cell. In Proceedings of the 2020 IEEE 20th Mediterranean Electrotechnical Conference (MELECON), Palermo, Italy, 16–18 June 2020; pp. 411–414.
217. Roth, C.C.; Tolstykh, G.P.; Payne, J.A.; Kuipers, M.A.; Thompson, G.L.; DeSilva, M.N.; Ibey, B.L. Nanosecond pulsed electric field thresholds for nanopore formation in neural cells. *J. Biomed. Opt.* **2013**, *18*, 035005. [CrossRef]
218. Vadlamani, R.A.; Nie, Y.; Detwiler, D.A.; Dhanabal, A.; Kraft, A.M.; Kuang, S.; Gavin, T.P.; Garner, A.L. Nanosecond pulsed electric field induced proliferation and differentiation of osteoblasts and myoblasts. *J. R. Soc. Interface* **2019**, *16*, 20190079. [CrossRef]
219. Zhang, K.; Guo, J.; Ge, Z.; Zhang, J. Nanosecond pulsed electric fields (nsPEFs) regulate phenotypes of chondrocytes through Wnt/β-catenin signaling pathway. *Sci. Rep.* **2014**, *4*, 5836. [CrossRef] [PubMed]

220. Morotomi-Yano, K.; Uemura, Y.; Katsuki, S.; Akiyama, H.; Yano, K. Activation of the JNK pathway by nanosecond pulsed electric fields. *Biochem. Biophys. Res. Commun.* **2011**, *408*, 471–476. [CrossRef] [PubMed]
221. Muratori, C.; Pakhomov, A.G.; Gianulis, E.; Meads, J.; Casciola, M.; Mollica, P.A.; Pakhomova, O.N. Activation of the phospholipid scramblase TMEM16F by nanosecond pulsed electric fields (nsPEF) facilitates its diverse cytophysiological effects. *J. Biol. Chem.* **2017**, *292*, 19381–19391. [CrossRef] [PubMed]
222. Beebe, S.J.; Blackmore, P.F.; White, J.; Joshi, R.P.; Schoenbach, K.H. Nanosecond pulsed electric fields modulate cell function through intracellular signal transduction mechanisms. *Physiol. Meas.* **2004**, *25*, 1077. [CrossRef]
223. Guo, S.; Jackson, D.L.; Burcus, N.I.; Chen, Y.J.; Xiao, S.; Heller, R. Gene electrotransfer enhanced by nanosecond pulsed electric fields. *Mol. Ther. Methods Clin. Dev.* **2014**, *1*, 14043. [CrossRef]
224. Estlack, L.E.; Roth, C.C.; Thompson, G.L.; Lambert, W.A.; Ibey, B.L. Nanosecond pulsed electric fields modulate the expression of Fas/CD95 death receptor pathway regulators in U937 and Jurkat Cells. *Apoptosis* **2014**, *19*, 1755–1768. [CrossRef]
225. Zhang, R.; Aji, T.; Shao, Y.; Jiang, T.; Yang, L.; Lv, W.; Chen, Y.; Chen, X.; Wen, H. Nanosecond pulsed electric field (nsPEF) disrupts the structure and metabolism of human Echinococcus granulosus protoscolex in vitro with a dose effect. *Parasitol. Res.* **2017**, *116*, 1345–1351. [CrossRef]
226. Chen, X.; Zhang, R.; Aji, T.; Shao, Y.; Chen, Y.; Wen, H. Novel interventional management of hepatic hydatid cyst with nanosecond pulses on experimental mouse model. *Sci. Rep.* **2017**, *7*, 4491. [CrossRef]
227. Chen, X.; Zhang, R.; Wen, H. Experimental nanopulse ablation of multiple membrane parasite on ex vivo hydatid cyst. *BioMed Res. Int.* **2018**, *2018*, 8497283 . [CrossRef]
228. Hargrave, B.; Li, F. Nanosecond pulse electric field activation of platelet-rich plasma reduces myocardial infarct size and improves left ventricular mechanical function in the rabbit heart. *J. Extra-Corpor. Technol.* **2012**, *44*, 198.
229. Xiao, S.; Kiyan, T.; Blackmore, P.; Schoenbach, K. Pulsed Power for Wound Healing. In Proceedings of the 2008 IEEE International Power Modulators and High-Voltage Conference, Las Vegas, NV, USA, 27–31 May 2008; pp. 69–72.
230. Hargrave, B.; Li, F. Nanosecond Pulse Electric Field Activated-Platelet Rich Plasma Enhances the Return of Blood Flow to Large and Ischemic Wounds in a Rabbit Model. *Physiol. Rep.* **2015**, *3*, e12461. [CrossRef] [PubMed]
231. Nuccitelli, R.; Berridge, J.C.; Mallon, Z.; Kreis, M.; Athos, B.; Nuccitelli, P. Nanoelectroablation of murine tumors triggers a CD8-dependent inhibition of secondary tumor growth. *PLoS ONE* **2015**, *10*, e0134364. [CrossRef] [PubMed]
232. Chen, R.; Sain, N.M.; Harlow, K.T.; Chen, Y.J.; Shires, P.K.; Heller, R.; Beebe, S.J. A protective effect after clearance of orthotopic rat hepatocellular carcinoma by nanosecond pulsed electric fields. *Eur. J. Cancer* **2014**, *50*, 2705–2713. [CrossRef] [PubMed]
233. Guo, S.; Jing, Y.; Burcus, N.I.; Lassiter, B.P.; Tanaz, R.; Heller, R.; Beebe, S.J. Nano-pulse stimulation induces potent immune responses, eradicating local breast cancer while reducing distant metastases. *Int. J. Cancer* **2018**, *142*, 629–640. [CrossRef]
234. Skeate, J.G.; Da Silva, D.M.; Chavez-Juan, E.; Anand, S.; Nuccitelli, R.; Kast, W.M. Nano-Pulse Stimulation induces immunogenic cell death in human papillomavirus-transformed tumors and initiates an adaptive immune response. *PLoS ONE* **2018**, *13*, e0191311. [CrossRef]
235. Nuccitelli, R.; Tran, K.; Lui, K.; Huynh, J.; Athos, B.; Kreis, M.; Nuccitelli, P.; De Fabo, E.C. Non-thermal nanoelectroablation of UV-induced murine melanomas stimulates an immune response. *Pigment Cell Melanoma Res.* **2012**, *25*, 618–629. [CrossRef]
236. Nuccitelli, R.; McDaniel, A.; Anand, S.; Cha, J.; Mallon, Z.; Berridge, J.C.; Uecker, D. Nano-Pulse Stimulation is a physical modality that can trigger immunogenic tumor cell death. *J. Immunother. Cancer* **2017**, *5*, 32. [CrossRef]
237. Nuccitelli, R.; Wood, R.; Kreis, M.; Athos, B.; Huynh, J.; Lui, K.; Nuccitelli, P.; Epstein, E.H., Jr. First-in-human trial of nanoelectroablation therapy for basal cell carcinoma: Proof of method. *Exp. Dermatol.* **2014**, *23*, 135–137. [CrossRef]
238. Garon, E.B.; Sawcer, D.; Vernier, P.T.; Tang, T.; Sun, Y.; Marcu, L.; Gundersen, M.A.; Koeffler, H.P. In vitro and in vivo evaluation and a case report of intense nanosecond pulsed electric field as a local therapy for human malignancies. *Int. J. Cancer* **2007**, *121*, 675–682. [CrossRef]
239. Mir, L.M.; Orlowski, S.; Belehradek, J., Jr.; Paoletti, C. Electrochemotherapy potentiation of antitumour effect of bleomycin by local electric pulses. *Eur. J. Cancer Clin. Oncol.* **1991**, *27*, 68–72. [CrossRef]
240. Serša, G.; Čemažar, M.; Miklavčič, D. Antitumor effectiveness of electrochemotherapy with cis-diamminedichloroplatinum (II) in mice. *Cancer Res.* **1995**, *55*, 3450–3455. [PubMed]
241. Ouyang, L.; Shi, Z.; Zhao, S.; Wang, F.T.; Zhou, T.T.; Liu, B.; Bao, J.K. Programmed cell death pathways in cancer: A review of apoptosis, autophagy and programmed necrosis. *Cell Prolif.* **2012**, *45*, 487–498. [CrossRef] [PubMed]
242. Salido, G.M.; Rosado, J.A. *Apoptosis: Involvement of Oxidative Stress and Intracellular Ca^{2+} Homeostasis*; Universty of Extremadure: Badajoz, Spain, 2009; pp. 229–235.
243. Stacey, M.; Stickley, J.; Fox, P.; O'Donnell, C.; Schoenbach, K.; Beebe, S.; Buescher, S. Increased cell killing and DNA damage in cells exposed to ultra-short pulsed electric fields. In Proceedings of the Electrical Insulation and Dielectric Phenomena, Cancun, Mexico, 20–24 October 2002; pp. 79–82.
244. Chen, X.; Zhuang, J.; Kolb, J.F.; Schoenbach, K.H.; Beebe, S.J. Long term survival of mice with hepatocellular carcinoma after pulse power ablation with nanosecond pulsed electric fields. *Technol. Cancer Res. Treat.* **2012**, *11*, 83–93. [CrossRef] [PubMed]
245. Nuccitelli, R.; Huynh, J.; Lui, K.; Wood, R.; Kreis, M.; Athos, B.; Nuccitelli, P. Nanoelectroablation of human pancreatic carcinoma in a murine xenograft model without recurrence. *Int. J. Cancer* **2013**, *132*, 1933–1939. [CrossRef]
246. Fulda, S.; Gorman, A.M.; Hori, O.; Samali, A. Cellular stress responses: Cell survival and cell death. *Int. J. Cell Biol.* **2010**, *2010*, 214074. [CrossRef]

247. Stacey, M.; Stickley, J.; Fox, P.; Statler, V.; Schoenbach, K.; Beebe, S.; Buescher, S. Differential effects in cells exposed to ultra-short, high intensity electric fields: Cell survival, DNA damage, and cell cycle analysis. *Mutat. Res. Toxicol. Environ. Mutagen.* **2003**, *542*, 65–75. [CrossRef]
248. Zhang, Y.; Dong, F.; Liu, Z.; Guo, J.; Zhang, J.; Fang, J. Nanosecond pulsed electric fields promoting the proliferation of porcine iliac endothelial cells: An in vitro study. *PLoS ONE* **2018**, *13*, e0196688.
249. Dong, F.; Liu, Z.; Zhang, J.; Fang, J.; Guo, J.; Zhang, Y. Nspefs Promoting the Proliferation of Piec Cells: An in Vitro Study. In Proceedings of the 2017 IEEE International Conference on Plasma Science (ICOPS), Atlantic City, NJ, USA, 21–25 May 2017; p. 1.
250. Guo, J.; Ma, R.; Su, B.; Li, Y.; Zhang, J.; Fang, J. Raising the avermectins production in Streptomyces avermitilis by utilizing nanosecond pulsed electric fields (nsPEFs). *Sci. Rep.* **2016**, *6*, 25949. [CrossRef]
251. Rajabi, F.; Gusbeth, C.; Frey, W.; Maisch, J.; Nick, P. Nanosecond pulsed electrical fields enhance product recovery in plant cell fermentation. *Protoplasma* **2020**, *257*, 1585–1594. [CrossRef]
252. Prorot, A.; Arnaud-Cormos, D.; Lévêque, P.; Leprat, P. Bacterial stress induced by nanosecond pulsed electric fields (nsPEF): Potential applications for food industry and environment. In Proceedings of the IV International Conference on Environmental, Industrial and Applied Microbiolog, Malaga, Spain, 14–16 September 2011.
253. Haberkorn, I.; Buchmann, L.; Häusermann, I.; Mathys, A. Nanosecond pulsed electric field processing of microalgae based biorefineries governs growth promotion or selective inactivation based on underlying microbial ecosystems. *Bioresour. Technol.* **2020**, *319*, 124173. [CrossRef]
254. Su, B.; Guo, J.; Nian, W.; Feng, H.; Wang, K.; Zhang, J.; Fang, J. Early growth effects of nanosecond pulsed electric field (nsPEFs) exposure on Haloxylon ammodendron. *Plasma Process. Polym.* **2015**, *12*, 372–379. [CrossRef]
255. Eing, C.J.; Bonnet, S.; Pacher, M.; Puchta, H.; Frey, W. Effects of nanosecond pulsed electric field exposure on Arabidopsis thaliana. *IEEE Trans. Dielectr. Electr. Insul.* **2009**, *16*, 1322–1328. [CrossRef]
256. Songnuan, W.; Kirawanich, P. Early growth effects on Arabidopsis thaliana by seed exposure of nanosecond pulsed electric field. *J. Electrost.* **2012**, *70*, 445–450. [CrossRef]
257. Suchomel, P.; Kvitek, L.; Panacek, A.; Prucek, R.; Hrbac, J.; Vecerova, R.; Zboril, R. Comparative study of antimicrobial activity of AgBr and Ag nanoparticles (NPs). *PLoS ONE* **2015**, *10*, e0119202. [CrossRef]
258. Vadlapudi, V.; Kaladhar, D.; Behara, M.; Sujatha, B.; Naidu, G.K. Synthesis of green metallic nanoparticles (NPs) and applications. *Orient. J. Chem* **2013**, *29*, 1589–1595. [CrossRef]
259. Boedeker, K.L.; Cooper, V.N.; McNitt-Gray, M.F. Application of the noise power spectrum in modern diagnostic MDCT: Part I. Measurement of noise power spectra and noise equivalent quanta. *Phys. Med. Biol.* **2007**, *52*, 4027. [CrossRef]
260. Dobbins, J.T., III; Samei, E.; Ranger, N.T.; Chen, Y. Intercomparison of methods for image quality characterization. II. Noise power spectrum a. *Med Phys.* **2006**, *33*, 1466–1475. [CrossRef]
261. Grisaffe, D.B. Questions about the ultimate question: Conceptual considerations in evaluating Reichheld's net promoter score (NPS). *J. Consum. Satisf. Dissatisfaction Complain. Behav.* **2007**, *20*, 36.
262. Baehre, S.; O'Dwyer, M.; O'Malley, L.; Lee, N. The use of Net Promoter Score (NPS) to predict sales growth: Insights from an empirical investigation. *J. Acad. Mark. Sci.* **2022**, *50*, 67–84. [CrossRef]
263. Melikov, K.C.; Frolov, V.A.; Shcherbakov, A.; Samsonov, A.V.; Chizmadzhev, Y.A.; Chernomordik, L.V. Voltage-induced nonconductive pre-pores and metastable single pores in unmodified planar lipid bilayer. *Biophys. J.* **2001**, *80*, 1829–1836. [CrossRef]
264. Vernier, P.T.; Sun, Y.; Gundersen, M.A. Nanoelectropulse-driven membrane perturbation and small molecule permeabilization. *BMC Cell Biol.* **2006**, *7*, 37. [CrossRef] [PubMed]
265. Vasilkoski, Z.; Esser, A.T.; Gowrishankar, T.; Weaver, J.C. Membrane electroporation: The absolute rate equation and nanosecond time scale pore creation. *Phys. Rev. E* **2006**, *74*, 021904. [CrossRef] [PubMed]
266. Pakhomov, A.G.; Miklavcic, D.; Markov, M.S. *Advanced Electroporation Techniques in Biology and Medicine*; CRC Press: Boca Raton, FL, USA, 2010.
267. Pakhomov, A.G.; Pakhomova, O.N. Nanopores: A distinct transmembrane passageway in electroporated cells. In *Advanced Electroporation Techniques in Biology in Medicine*; CRC Press: Boca Raton, FL, USA, 2010, pp. 178–194.
268. Bowman, A.M.; Nesin, O.M.; Pakhomova, O.N.; Pakhomov, A.G. Analysis of plasma membrane integrity by fluorescent detection of Tl+ uptake. *J. Membr. Biol.* **2010**, *236*, 15–26. [CrossRef] [PubMed]
269. Ibey, B.L.; Pakhomov, A.G.; Gregory, B.W.; Khorokhorina, V.A.; Roth, C.C.; Rassokhin, M.A.; Bernhard, J.A.; Wilmink, G.J.; Pakhomova, O.N. Selective cytotoxicity of intense nanosecond-duration electric pulses in mammalian cells. *Biochim. Biophys. Acta (BBA)-Gen. Subj.* **2010**, *1800*, 1210–1219. [CrossRef]
270. LITJTER, J.; JD, L. Stability of lipid bilayers and red blood cell membranes. *Phys. Lett. A* **1975**, *53*, 193–194. [CrossRef]
271. Brochard-Wyart, F.; de Gennes, P.G.; Sandre, O. Transient pores in stretched vesicles: Role of leak-out. *Phys. A Stat. Mech. Appl.* **2000**, *278*, 32–51. [CrossRef]
272. Leontiadou, H.; Mark, A.E.; Marrink, S.J. Molecular dynamics simulations of hydrophilic pores in lipid bilayers. *Biophys. J.* **2004**, *86*, 2156–2164. [CrossRef]
273. Jiang, F.Y.; Bouret, Y.; Kindt, J.T. Molecular dynamics simulations of the lipid bilayer edge. *Biophys. J.* **2004**, *87*, 182–192. [CrossRef]
274. Gianulis, E.C.; Labib, C.; Saulis, G.; Novickij, V.; Pakhomova, O.N.; Pakhomov, A.G. Selective susceptibility to nanosecond pulsed electric field (nsPEF) across different human cell types. *Cell. Mol. Life Sci.* **2017**, *74*, 1741–1754. [CrossRef]

275. Li, Y.C.; Park, M.J.; Ye, S.K.; Kim, C.W.; Kim, Y.N. Elevated levels of cholesterol-rich lipid rafts in cancer cells are correlated with apoptosis sensitivity induced by cholesterol-depleting agents. *Am. J. Pathol.* **2006**, *168*, 1107–1118. [CrossRef]
276. Merchant, T.E.; Kasimos, J.N.; Vroom, T.; de Bree, E.; Iwata, J.L.; de Graaf, P.W.; Glonek, T. Malignant breast tumor phospholipid profiles using 31P magnetic resonance. *Cancer Lett.* **2002**, *176*, 159–167. [CrossRef]
277. Sterin, M.; Cohen, J.S.; Ringel, I. Hormone sensitivity is reflected in the phospholipid profiles of breast cancer cell lines. *Breast Cancer Res. Treat.* **2004**, *87*, 1–11. [CrossRef] [PubMed]
278. Dória, M.L.; Cotrim, Z.; Macedo, B.; Simões, C.; Domingues, P.; Helguero, L.; Domingues, M.R. Lipidomic approach to identify patterns in phospholipid profiles and define class differences in mammary epithelial and breast cancer cells. *Breast Cancer Res. Treat.* **2012**, *133*, 635–648. [CrossRef] [PubMed]
279. Dória, M.L.; Cotrim, C.Z.; Simões, C.; Macedo, B.; Domingues, P.; Domingues, M.R.; Helguero, L.A. Lipidomic analysis of phospholipids from human mammary epithelial and breast cancer cell lines. *J. Cell. Physiol.* **2013**, *228*, 457–468. [CrossRef]
280. Patra, S.K. Dissecting lipid raft facilitated cell signaling pathways in cancer. *Biochim. Biophys. Acta (BBA)-Rev. Cancer* **2008**, *1785*, 182–206. [CrossRef]
281. Niemelä, P.S.; Ollila, S.; Hyvönen, M.T.; Karttunen, M.; Vattulainen, I. Assessing the nature of lipid raft membranes. *PLoS Comput. Biol.* **2007**, *3*, e34. [CrossRef]
282. Lingwood, D.; Simons, K. Lipid rafts as a membrane-organizing principle. *Science* **2010**, *327*, 46–50. [CrossRef]
283. Staubach, S.; Hanisch, F.G. Lipid rafts: Signaling and sorting platforms of cells and their roles in cancer. *Expert Rev. Proteom.* **2011**, *8*, 263–277. [CrossRef]